CJC Chinese Journal of Chemistry 中国化学 - An International Journal

For submission: https://mc.manuscriptcentral.com/cjoc
For published articles: https://onlinelibrary.wiley.com/journal/16147065

Recent Advances

Cite this paper: *Chin. J. Chem.* **2023**, *41*, 3050—3062. **DOI: 10.1002/cjoc.202300191**

Engineering Colloidal Metal-Semiconductor Nanorods Hybrid Nanostructures for Photocatalysis†

Jiayi Chen,[a] Derek Hao,[b] Wei Chen,[a] Yazi Liu,[c] Zongyou Yin,[d] Hsien-Yi Hsu,*[,e] Bing-Jie Ni,*[,b] Aixiang Wang,*[,f] Simon W. Lewis,[a] and Guohua Jia*[,a]

[a] *School of Molecular and Life Sciences, Curtin University, Bentley, Perth WA, 6102, Australia*
[b] *Centre for Technology in Water and Wastewater, School of Civil and Environmental Engineering, University of Technology Sydney, Ultimo, NSW 2007, Australia*
[c] *School of the Environment, Nanjing Normal University, Nanjing, Jiangsu 210046, China*
[d] *Research School of Chemistry, The Australian National University, ACT 2601, Australia*
[e] *School of Energy and Environment & Department of Materials Science and Engineering, City University of Hong Kong, Kowloon Tong, Hong Kong, China, and Shenzhen Research Institute of City University of Hong Kong, Shenzhen, 518057, China*
[f] *School of Chemistry and Chemical Engineering, Linyi University, Linyi, Shandong 276005, China*

Keywords

Hybrid nanostructure | Metal-semiconductor nanorod | Engineering strategy | Photocatalysis | Hydrogen production

Comprehensive Summary

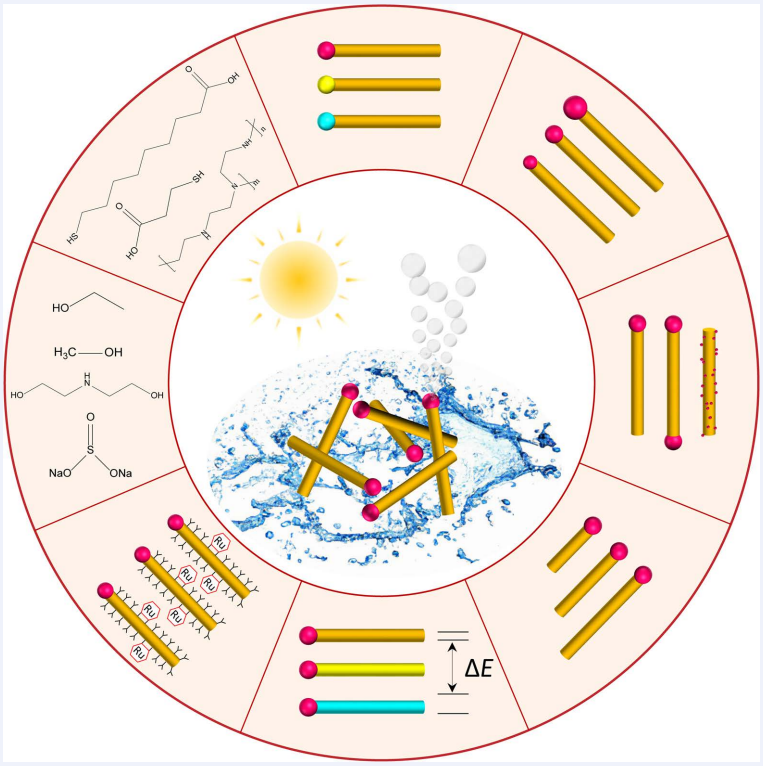

Emerging engineering strategies of colloidal metal-semiconductor nanorod hybrid nanostructures spanning from type, size, dimension, and location of both metal nanoparticles and semiconductors, co-catalyst, band gap structure, surface ligand to hole scavenger are elaborated symmetrically to rationalize the design of this type of intriguing materials for efficient photocatalytic applications.

*E-mail: sam.hyhsu@cityu.edu.hk; bingjieni@gmail.com; wangaixiang1974@163.com; guohua.jia@curtin.edu.au

† Dedicated to the Special Issue of Energy Materials.

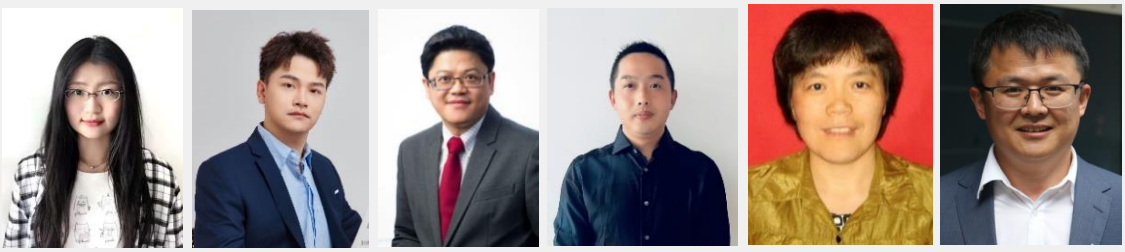

Left to Right: Jiayi Chen, Derek Hao, Hsien-Yi Hsu, Bingjie Ni, Aixiang Wang, and Guohua Jia

Jiayi Chen is a PhD student under the supervison of Dr. Guohua Jia at Curtin University. Her research focuses on the development of colloidal semiconductor nanocrystals for optoelectronic and photocatalytic applications.

Dr. Derek Hao obtained bachelor degree in materials science in 2017 from China University of Geosciences Beijing. He then obtained his PhD from Centre for Technology in Water and Wastewater, University of Technology Sydney in 2021 and subsequently joined Griffith University as a research fellow. In 2022, he was awarded the prestigious Humboldt Research Fellowship and started to work at Max Planck Institute of Colloids and Interfaces. His research mainly focuses on the nanomaterials and nanotechnology for wastewater treatment and clean energy generation.

Dr. Hsien-Yi Hsu is an Assistant Professor in the School of Energy and Environment at City University of Hong Kong. He obtained his PhD degree under supervision of Prof. Kirk S. Schanze at University of Florida. After that, he received the two-year postdoctoral and research associate's appointments respectively with Prof. Allen J. Bard and Prof. Edward T. Yu in Center for Electrochemistry as well as Department of Electrical and Computer Engineering at University of Texas at Austin. The area of his expertise stretches from material design to new related disciplines involving material characterization and diverse applications, such as solar fuels, organic and inorganic photovoltaic cells, wastewater treatment and food waste management.

Prof. Bing-Jie Ni received his PhD degree in environmental engineering in June 2009. He currently is an ARC Future Fellow and full professor at University of Technology Sydney. He has been working in the field of environmental technology and water management, focusing on the integration of these disciplines to develop innovative and sustainable technological solutions to achieve high-levels of pollutant removal with minimised carbon emissions. He has published more than 400 refereed journal papers with over 20000 citations and an H-index of 77. He is also a Clarivate Highly Cited Researcher.

Aixiang Wang is a professor in the School of Chemistry and Chemical Engineering at Linyi University, China. She obtained her PhD from Northwest Normal University in 2008. Her research interests focus on the synthesis and application of inorganic materials.

Guohua Jia is an associate professor at Curtin University, Australia. He obtained his Ph.D. degree in chemistry in 2009 from City University of Hong Kong. Then he had been working as a postdoctoral fellow with Prof. Uri Banin at the Hebrew University of Jerusalem, Israel from 2010 to 2014. He commenced his current role as a group leader at Curtin University in 2015. His research interests focus on chemistry and physics of colloidal nanocrystals, with particular emphasis on their shape-dependent properties and applications in catalysis and optoelectronic devices.

Contents

1. Introduction 3051
2. Synthetic Approaches 3051
   2.1. Surface nucleation 3052
   2.2. Materials diffusion 3052
   2.3. Solution-liquid-solid method 3053
3. Engineering Strategies 3053
   3.1. Types of metal nanoparticles and semiconductors 3053
   3.2. Size of metal domain 3054
   3.3. Surface location of metal nanoparticles 3055
   3.4. Length of nanorods with respect to the core 3056
   3.5. Solution-liquid-solid method 3056
   3.6. Band gap structure 3057
   3.7. Surface ligands 3057
   3.8. Hole scavenger 3058
   3.9. Other strategies nanorods 3059
4. Conclusion and Outlook 3059

1. Introduction

Colloidal semiconductor nanorods manifest size- and shape-depended properties, large absorption cross-section, and improved charge transport and separation.[1] The integration of metal particles with semiconductor nanorods produces a new type of materials, *i.e.*, hybrid nanords, with enhanced charge separation capabilities with relevance to applications in photocatalysis.[2] In the metal-semiconductor nanorods hybrid nanostructures, 1D semiconductor nanorods typically have a length from a few nanometers to a few hundred nanometers, with a diameter ranging from 1 nm to about 50 nm. For the metal domain, it can be extremely small nanoclusters, or nanocrystals ranging from a few nanometers to a dozen nanometers in diameter. The role of metal-semiconductor hybrid nanorods in photocatalysis is explained by the light absorption and the formation of electron-hole pairs in semiconductor domain and by charge separation on metal-semiconductor nanojunctions.[3] Efficient charge separation on the metal-semiconductor nanorods makes it possible to serve as a photocatalyst for hydrogen production from water splitting, which is a hot topic in the research of hybrid nanomaterials.[4]

Although the syntheses,[5a-b] architectures,[5c] plasmonic properties[5d] and catalytic properties[2a,5e] of hybrid nanocrystals have been reviewed in a couple of prominent review papers, none of above specifically targets one-dimensional (1D) metal-semiconductor nanorods hybrid nanostructures. Furthermore, to the best of our knowledge, the engineering of the metal-semiconductor nanocrystals hybrid nanostructures, especially for anisotropic nanorods with elongated shape, has not been appropriately compared and summarized so far. Thus, it is highly demanded to composite a review paper to outline the emerging engineering strategies of such hybrid nanostructures with tailored properties to boost photocatalysis and to provide insightful perspectives on this stimulating research area. Here, we contribute a timely review to rationalize the design of metal-semiconductor nanorods hybrid nanostructures through the engineering strategies to maximize their full potential in photocatysis. This review consists of a brief introduction to the synthetic approaches of metal-semiconductor nanorods hybrid nanostructures followed by a broad scope of engineering strategies, including types of metal and semiconductor components, size and growth location of metal nanoparticles, dimensional of semiconductor nanorods, types of co-catalyst, band gap structures, surface ligands, hole scavengers and other strategies. Finally, the challenges and future perspectives for metal-semiconductor nanorods hybrid nanostructures are proposed.

2. Synthetic Approaches

The in-depth understanding of the growth mechanisms and

state-of-the-art wet-chemical synthetic methods make it possible to prepare colloidal metal-semiconductor hybrid nanorods with diverse architectures in a predefined manner. In this section, three typical synthetic methods such as surface nucleation (Figure 1A), material diffusion (Figure 2A), and solution-liquid-solid (SLS) growth (Figure 3A) with representative examples have been reviewed to provide general background information on the controlled synthesis of the metal-semiconductor nanorods hybrid nanostructures. To have a comprehensive understanding of the synthesis of metal-semiconductor hybrid nanorods, Table 1 was used to summarize the synthesis methods and conditions of metal-semiconductor hybrid nanorods.

Table 1 Comparison of synthesis methods and conditions of metal-semiconductor hybrid nanorods

Synthesis Approach	Compound	Engineering strategy	Reaction temperature	Surfactant	Ref.
Surface nucleation	Au-CdSe	Length of nanorods	Room temperature	Dodecylamine	[6b]
Surface nucleation	Pt-CdS	Surface location of metal domain	Room temperature	Triethylamine	[6c]
Surface nucleation	Au-CdS	Surface location of metal domain	0, 20 or 40 ℃	Dodecylamine, octadecylamine or trioctylamine	[6d]
Material diffusion	Au-CdSe	Surface location of metal domain	Room temperature	octylamine	[7]
Solution-liquid-solid	Ag-ZnS	Size of metal domain	180—220 °C	1-Dodecanethiol	[9]

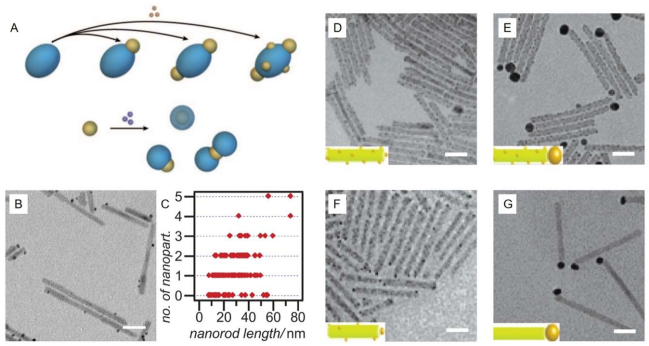

Figure 1 A) Schemes of growth of metal phase at different positions of semiconductor nanoparticles (top) and growth of semiconductor on the metal nanoparticle (bottom). B) Transmission electron microscopy (TEM) image of Pt-CdS heterostructure, the scale bar is 20 nm. C) The number of Pt nanocrystals on a CdS nanorod as a function of its length. t = 120 min. D—G) Au nanocrystals growth on CdS nanorods for 1 h: D) 313 K, dark, E) 313 K, 473 nm laser irradiation, F) 273 K, dark and G) 273 K, 473 nm laser irradiation, the scale bar is 20 nm. A) Reproduced with permission.[5e] Copyright 2010, Wiley-VCH. B—C) Reproduced with permission.[6c] Copyright 2008, Wiley-VCH. D—G) Reproduced with permission.[6d] Copyright 2009, American Chemical Society.

2.1. Surface nucleation

As a widely used method for the preparation of the metal-semiconductor nanorods hybrid nanostructures, the process of surface nucleation usually needs some external inputs such as light illumination or heat in combination with the presence of concentrated precursors and surface binding ligands to facilitate the nucleation of metals on semiconductor nanocrystals. This is because the energy barrier for the nucleation of the metal onto the semiconductor nanocrystals could be overcome by an external input in the form of light illumination or heat.[6] Mokari *et al.* performed site-selective growth of Au on CdSe nanorods at room temperature. As the end facets of nanorods are less passivated by surfactant and have increased surface energy, Au tends to grow on the tips of nanorods.[6b] Dukovic *et al.* reported the photodeposition of Pt on colloidal CdS nanorods (Figure 1B).[6c] They found that Pt randomly distributed along the nanorod length with no preference for rod ends. This finding is different from metal-chalcogenide hybrid nanostructures synthesized by thermal methods wherein metal preferably deposits on the end of nanorods forming match-like or dumbbell-like heterostructures. Many nanorods, even some of them are longer than 50 nm, have no indication of any Pt deposition (Figure 1C). This may be because metal deposition requires the presence of surface defects or incomplete surface passivation sites on the nanorods as carrier traps. Menagen *et al.* studied the effects of light and temperature on the surface nucleation process of Au on CdS nanorods.[6d] As shown in Figures 1D—G, Au grew on CdS nanorods under different conditions. The results showed that Au can grow on the sulfur-ended facet of the nanorods when exposed to light, and surface defect growth can be suppressed at low temperatures (almost completely inhibited at 273 K), owing to the adsorption of more ligands onto the CdS nanorods and passivating of the surface, thus preventing defect growth. Therefore, the size and growth location of metal domain can be easily controlled through surface passivation and elaboration of synthesis conditions.[6d]

2.2. Materials diffusion

The driving force of Ostwald ripening comes from the interface energy which tends to reach its lowest value under thermodynamic conditions. As the larger particles grow at the expense of the smaller particles, the specific interface energy per unit mass decreases, while the total free energy of the system is reduced.[5e] This mechanism can be used in the design and fabrication of metal-semiconductor hybrid nanostructures. Bala *et al.* used this mechanism for surface diffusion growth. The phase transfer of $AuCl_4^-$ and subsequent metal reduction were carried out using a water-soluble $HAuCl_4$ precursor and octylamine, and Au was grown to the tip of the CdSe nanorod. Initially, as shown in Figure 2B, several small Au particles were found on CdSe nanorods like gold islands, not only at the tip but also on the body of the rod. After 4 h, it was found that all the small gold islands on the CdSe were aggregated at one end of the nanorods and became bigger (Figure

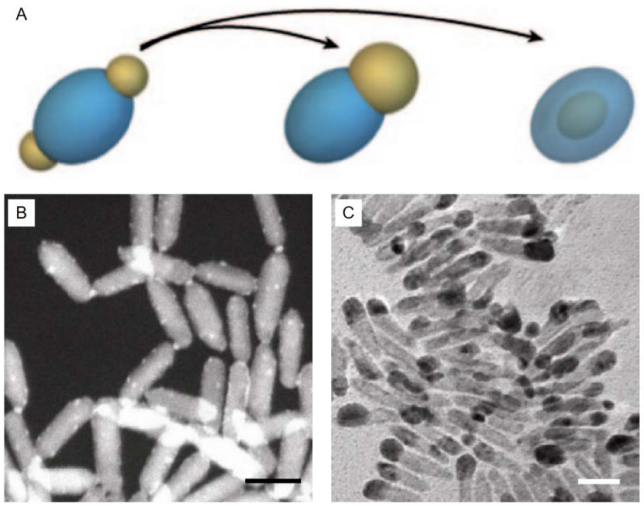

Figure 2 A) Schemes of surface diffusion (middle) or inward diffusion (right) of the metal phase after surface nucleation. B) Scanning transmission electron microscopy (STEM) image of the CdSe-Au heterostructure after 1 h of reaction. C) TEM image of CdSe-Au heterostructure after 4 h of reaction. The scale bar is 20 nm. A) Reproduced with permission.[5e] Copyright 2010, Wiley-VCH. B—C) Reproduced with permission.[7] Copyright 2013, Tsinghua University Press and Springer-Verlag Berlin Heidelberg.

2C). The metal tip size can be adjusted through controlling the nucleation time and growth rate of the gold islands at different locations during the growth process. Under the Ostwald ripening mechanism, when the size of each Au nanoparticle reaches thermodynamic stability, the smaller tip will gradually be oxidized and dissolved into the solvent, and electrons will be transferred from the surface of the nanorod to the Au-tip, thereby continuing to produce Au and making the nanoparticles grow at one end.[7] Therefore, the metal-semiconductor hybrid structure with diverse metal domain size and growth location can be achieved.

2.3. Solution-liquid-solid method

SLS method is a facile synthetic approach for hybrid nanorods using the pre-synthesized metal nanoparticles. In this process, metal nanoparticles with low melting points introduced in the organic solvent are transformed into liquid metal clusters as a catalyst on which nanocrystals are precipitated, and the growth of crystals on metal droplets occurs only at the interface between them.[1f,8] Being different from the methods of surface nucleation and materials diffusion which require careful control of synthesis conditions, the ease and robustness of this method open new opportunities for the preparation of high quality 1D hybrid nanostructures with relevance in photocatalytic applications.[1f, 8d] Shen *et al.* prepared Ag-ZnS nanorods by the SLS method (Figures 3B, 3C) by optimizing the diameter of Ag nanocrystals, the concentration of Zn precursor, reaction time, reaction temperature and other conditions to effectively control the diameter and length of Ag-ZnS nanorods hybrid nanostructures.[9]

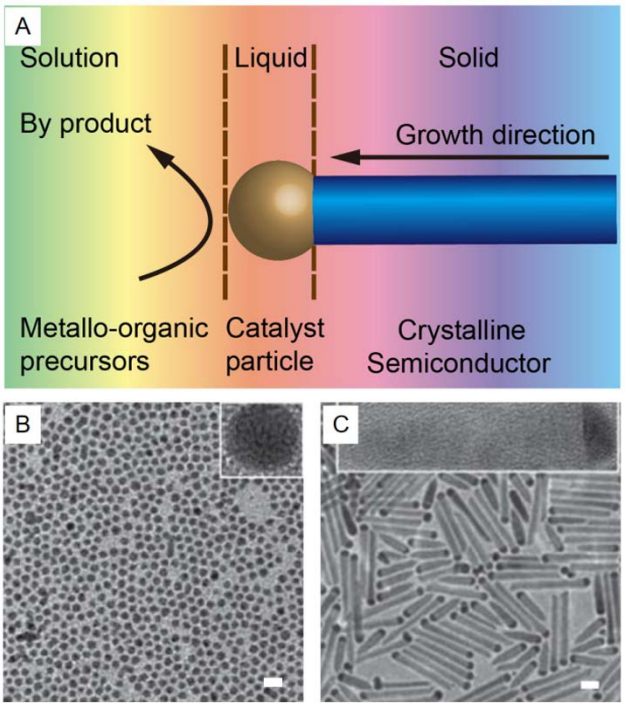

Figure 3 A) Scheme of 1D nanocrystals growth by the SLS method. B—C) TEM images of B) Ag nanoparticles (the inset is its high magnification image), C) Ag-ZnS hybrids (the inset is its high-magnification image). The scale bar is 20 nm. A) Reproduced with permission.[1f] Copyright 2019, Wiley-VCH. B—C) Reproduced with permission.[9] Copyright 2012, The Royal Society of Chemistry.

In summary, both surface nucleation and material diffusion methods allow for modulation of each domain in a typical metal-semiconductor heterostructural synthesis, enabling the application of different engineering strategies (discussed in detail in the next section). However, these two methods need multiple steps to realize the formation of the desired hybrid structures, and the synthesis of some hybrid structures by material diffusion method requires a long reaction time. As for the SLS method, it is a relatively simple and facile approach to prepare hybrid nanorods and crystal growth occurs only at the metal-semiconductor interface. Thus the morphology of the formed semiconductor is expected to be one-dimensional. However, there are few low melting point metals that can be selected as metal domains, which may hinder the exploration of metal-semiconductor hybrid structures with different compositions and limit the synthesis of catalysts with high catalytic properties.

3. Engineering Strategies

Metal-semiconductor hybrid nanoparticles are composed of at least two components made from different materials and exhibit not only unique characteristics that are intrinsic to each component but also new properties that are not possessed by each component due to synergistic effects. State-of-art synthetic approaches enable the precise control of the size, shape, composition and spacial location of metal-semiconductor hybrid nanorods so one can regulate their functionalities through the engineering strategies to realize their full potential in photocatalysis. At present, engineering strategies for leveraging the photocatalytic activity of metal-semiconductor hybrid nanoparticles mainly include changing metal types, adjusting the metal domain size, growing metal nanoparticles in different locations, adjusting the length of nanorods, introducing of co-catalyst, regulating band gap structure, using various type of surface ligands or hole scavenger, and so on. In this section, we will discuss and summarize the emerging engineering strategies.

3.1. Types of metal nanoparticles and semiconductors

Metal-semiconductor hybrid nanorods can be used as efficient catalysts for photocatalytic hydrogen evolution processes due to the enhanced charge separation capability and the reduction of the activation energy for the formation of hydrogen in a photocatalytic water splitting reaction. In the hybrid nanorods, the photoexcited electron generated by the light absorption of semiconductor is transferred to the metal domain to promote the water reduction reaction of hydrogen evolution. Each type of metals has different Fermi energy levels with diverse capabilities in separating charges and facilitating electrons to be transferred to the metal domain, so that metal-semiconductor hybrid nanorods may have diverse photocatalytic activities in hydrogen production.[10] Figure 4A is a schematic diagram of the Fermi energy levels of metals and band alignments of CdS. As shown in the Figure 4A, platinum has a relatively good reductive activity among these metals for catalytic water splitting reaction and has been widely studied.

Stone *et al.* prepared pristine CdS nanorods, hybrid Au-CdS and Pt-CdS heterostructures and compared their photocatalytic activities (Figures 4C and D).[11] The kinetics of hydrogen generation measured by gas chromatography showed that the hydrogen evolution efficiency of Pt-CdS hybrid nanorods was higher than that of Au-CdS hybrid nanorods, and both of them were larger than the bare CdS nanorods which is consistent with our previous discussion. Besides, they revealed that hydrogen peroxide and hydroxyl radical are produced more effectively by Au-tipped hybrid nanorods, which can be explained by d-band theory. Compared to the fully occupied d-band of Au metal, Pt tends to form strong Pt—O bond thus improves the dissociation of O—O bond. Tongying *et al.* performed hydrogen production by using CdSe/CdS and Pt-CdSe/CdS hybrid nanoparticles. Under broadband (UV/Visible) illumination, an obvious improvement of hydrogen production efficiency of Pt-CdSe/CdS hybrid nanoparticles can be clearly seen, and the hydrogen production rate is increased to 434.29 μmol h^{-1} g^{-1} from 80.92 μmol h^{-1} g^{-1} when Pt metal is introduced into the CdSe/CdS nanorods that forms Pt-CdSe/CdS hybrid nanoparticles.[12] Like other noble metals with excellent

hydrogen evolution performances, Pd is considered to be an efficient catalyst for hydrogen production in previous research.[10h] However, Aronovitch *et al.* shows that the efficiency of Pd-CdS/CdSe photocatalyst for hydrogen production is not such satisfactory, which is even worse than the Au-tipped hybrid nanorods due to the severe etching of nanorods (shortened about 21%) during Pd deposition process in its deposition process.[13] In this process, partial substitution of Cd ions by Pd ions in the nanorods produces more defect sites on the surface of the nanorods and consequently reduces the photocatalytic efficiency (Figure 4E). Furthermore, this type of hybrid nanorods is more likely to break down in the photocatalytic process.[13]

Bimetallic or polymetallic components sometimes can achieve better catalytic activity than single metal-based hybrid nanorods due to the increased adjustability of the catalyst properties, optimized width and energy position of the surface *d* band, and the synergistic effect.[14] Aronovitch *et al.* synthesized Au@Au/Pd tip CdS/CdSe nanorods (Figure 4F), which greatly improved hydrogen generation efficiency.[13] This is attributed to a more favorable hydrogen release at the bimetallic tip. On the other hand, Pd tends to form oxidation layer on the surface which increases the time of light induction, while more inert Au can reduce the formation of it. In addition, Au reduces migration of Pd by forming a physical barrier, making the structure of hybrid nanorods less susceptible to change than Pd tip nanorods.[13] Kalisman *et al.* prepared a combination of the same nanorods with different metal tips (Figure 4G). The results show that when the Pt is coated on the outside of the Au tip to form the Au@Pt core-shell structure, the hydrogen generation rate is twice as high as that of pure Pt-tipped hybrid nanorods. This can probably attributed to the fast injection of photoexcited electrons to Au and the ability of fully extraction of photoexcited electrons of Pt. When photodeposition of Au and Pt is carried out simultaneously on the nanorods, a gold core decorated with a platinum island is formed, which has a hydrogen generation rate four times higher than that of the pure Pt tip. It is believed that many exposed interfaces introduced between the two phases can achieve improved hydrogen evolution activity.[15]

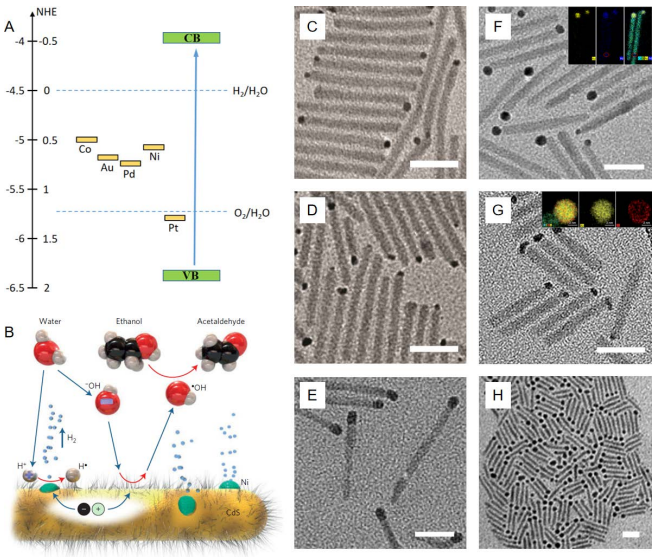

Figure 4 A) Scheme of the potentials of hydrogen evolution and oxygen evolution, bandgap of CdS semiconductor, and Fermi levels of each metal. B) Scheme of hole shuttle mechanism for the photocatalytic evolution of H_2, nickel nanoparticles growth on the cysteine-stabilized CdS nanorods for photocatalytic hydrogen generation, the photoexcited holes oxidize hydroxyl anions which act as a radical-carry away the positive charges, and in turn oxidize ethanol to acetaldehyde. The blue and red arrows show the movement of the species and a redox reaction respectively. TEM images of C) Au-CdS (2.5±0.6 nm), and D) Pt-CdS (1.9±0.5 nm) hybrid nanorods, respectively. The dimensions of CdS nanorods are 48±5 nm×3.3±0.5 nm. E) TEM images of Pd-CdS hybrids. F) TEM image of Au@Alloy-CdS hybrid nanorods (insets: from left to right are EDS elemental maps of Au, Pd, and an overlay of Cd, S, Au, and Pd). G) TEM image of bimetallic tips Au-Pt-CdSe@CdS hybrid nanorods (insets: EDS elemental maps of the bimetallic tip). H) TEM images of Co-CdSe hybrids after 24 h reaction at 80 °C. The scale bar of TEM images above are 20 nm. A) Reproduced with permission.[10i] Copyright 2018, The Royal Society of Chemistry. B) Reproduced with permission.[4d] Copyright 2014, Macmillan Publishers Limited. C—D) Reproduced with permission.[11] Copyright 2018, Wiley-VCH. E—F) Reproduced with permission.[13] Copyright 2016, American Chemical Society. G) Reproduced with permission.[15] Copyright 2015, The Royal Society of Chemistry. H) Reproduced with permission.[16] Copyright 2009, Wiley-VCH.

Generally speaking, noble metals can better extract charge for redox reaction at metal domain. However, it is difficult to achieve high-scale production due to the high cost of precious metals. Therefore, it is a trend of current research to seek abundant metal elements in the earth's crust as the metal components for metal-semiconductor hybrid nanorods. The non-noble metal elements that are currently studied are nickel, cobalt, *etc*. Simon *et al.* firstly used the Ni decorated CdS nanorods for visible light photocatalysis and they proposed a two-step mechanism to promote hole transfer from CdS to the hole scavenger by a hydroxyl anion/radical redox shuttle to improve the efficiency of hydrogen evolution.[4d] The basic principle of the process is shown in the Figure 4B. In Ni-CdS hybrid nanorods, an external quantum yield of up to 53% and internal quantum yield up to 71% at high $^{-}$OH ion concentrations with the system prevented photooxidation at a high pH are achieved.[4d] Maynadié *et al.* reported an example of heterogeneous growth of Co on CdSe nanorods (Figure 4H). With a Fermi level similar to Au, the band alignment of such hybrid nanorods will allow the transfer of electrons from the excited semiconductor to the metal tip within a shortened time period, which is consistent with the PL quenching observations in the photophysical studies. Due to ferromagnetism of Co, this type of hybrid nanorods are more commonly used in biological labelling and optoelectronic devices.[16]

3.2. Size of metal domain

As an important component to separate excitons, extract electrons and undergo reduction reaction, the size of the metal domain is one of the most important parameters for obtaining the optimal catalytic activity in the metal-semiconductor hybrid structure. Early studies show the Fermi level shifting of metal domain is caused by size decreasing which could affect catalytic performance of hybrid materials directly, the quantum size effect will also bring the adjustable semiconducting properties when the size of metal tip becomes tiny clusters. On the other hand, the undesired radiative recombination might occur on the metal clusters as well as the non-radiatively exciton recombination needs to be considered in the hybrid structure.[17]

Ben-Shahar *et al.* found that CdS-Au hybrid nanorods with large Au tips of a diameter of 7.1 ± 0.8 nm (Figure 5B) can better facilitate the separation and transference to metal domains of multiple excitons generated by high excitation fluence than small Au-tipped (1.5 ±0.2 nm) hybrid nanorods (Figure 5A). Figure 5C compares the quantum yield (QY) ratio of the large-tip to small-tip hybrid nanorods, indicating that the small tip favors hydrogen evolution in the single exciton region, while in the multi-exciton region this ratio drops sharply to near 1 : 1. This is mainly attributed to the transcendence of Auger recombination over electron transfer from the semiconductor to the metal tip for small tip hybrid nanorods, resulting in the loss of most of the excited electrons. Although increasing the intensity of excitons at the initial

stage of excitation can improve the QY, it eventually reduces the QY in the small-tip hybrid nanorods. For large-tip hybrid nanorods, the photocatalytic performance can be enhanced distinctly because the ultrafast electron transfer plays a dominant role than the Auger recombination and can extract all the excited electrons.[18] Nakibli *et al.* prepared CdSe@CdS hybrid nanorods with different sizes of Ni tips, and the characterizations showed that the lowest emission QY, maximum amplitude value (amplitude reflected charge transfer probability) and the faster depopulation process of conduction band were obtained on the 5.2 nm-sized Ni tips, which is consistent with the results of the highest quantum efficiency achieved at this size (Figure 5D).[19] This is reasonable given the fact that the two processes of Coulomb blockage, which has a greater influence on the small-tip, and the Schottky barrier height, which affects the large-tip more, compete with each other, thereby producing an optimum radius in the middle.[19] Selective small metal island growth on the CdS nanorods was obtained by varying the irradiation time and the Au^{3+}/nanorod ratio. Figure 5E (blue curve) shows the relationship between hydrogen production rate and Au tip size. The weak dependence observed on the two smallest dimensions while the photocatalytic performance of the larger Au domain is significantly reduced. Figure 5F shows the non-monotonic relationship between QY and Au tip sizes which is consistent with the standardized experiment QY (dotted line connected square). The opposite behavior of QY at the small and large size of Au domain could be attribute to the different main factors influencing the charge transfer rate. For the former, the precipitation of hydrogen QY is mainly determined by the electron injection rate at the metal tip, while on the larger Au tips the water reduction on the metal surface will play the dominant role. Therefore, the intermediate Au tip size provides the best balance between charge separation rate and efficiency.[20]

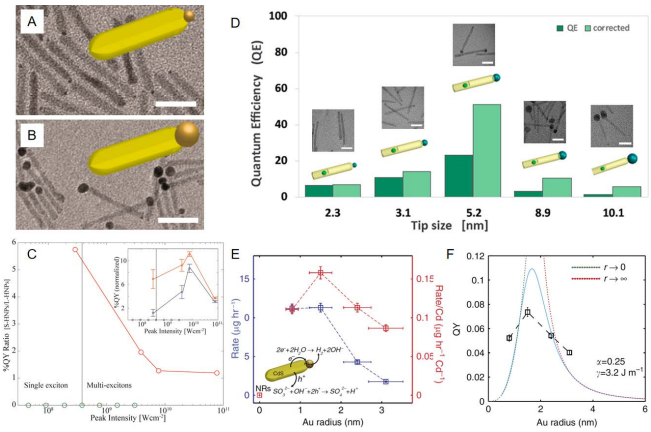

Figure 5 TEM images of A) CdS-Au hybrid nanorods with 1.5±0.2 nm and B) 7.1 ± 0.8 nm Au tip. C) Hydrogen evolution efficiencies ratio between small-tipped and large-tipped heterostructures as a function of excitation fluence presented as peak intensity of the irradiation beam (red circles) (inset: normalized hydrogen generation %QY of small-tipped hybrids (red) and the large-tipped hybrids (blue) as a function of excitation fluences presented as peak intensity of the irradiation beam. Green circles represent the corresponding peak intensities used in the TA experiments). D) Photocatalytic quantum efficiency for the water reduction of Ni-CdSe@CdS hybrids with different tip size. Experimental quantum efficiency in dark green bars, and the light green bars are quantum efficiency corrected for metal absorption. The insets are the TEM images of corresponding Ni-CdSe@CdS nanorods, from left to right: 2.3 nm, 3.1 nm, 5.2 nm, 8.9 nm, and 10.1 nm. E) Hydrogen production rate (blue) and Cd normalized rate (red) curves as a function of Au size domain in the hybrid nanoparticles. Negligible rates are measured for the CdS nanorods. The red curve is normalized to total Cd content to better express the basic metal size effect during hydrogen reduction. F) Measured QY (black dashed line) along with the non-monotonic kinetic model behaviour (blue solid line). Green and red dotted lines present limiting behaviours of the model for zero and infinite metal domain sizes, respectively. Error bars show the size distribution of the Au tip and the hydrogen production rate uncertainty. The scale bar is 20 nm. A—C) Reproduced with permission.[18] Copyright 2018, American Chemical Society. D) Reproduced with permission.[19] Copyright 2017, American Chemical Society. E-F) Reproduced with permission.[20] Copyright 2015, Springer Nature.

3.3. Surface location of metal nanoparticles

The place where metal was decorated on the semiconductor nanorods also affects the catalytic performances of the photocatalysts, owing to the variation of the rate of charge transfer and effectiveness of electron-hole separation. Besides, the loading in different positions will change the amount of metal requirements, which can affect the cost of the noble metal-semiconductor photocatalyst.[21]

Nakibli *et al.* proposed a general rule for the establishment of a catalytic system, that is, in the catalysis of multi-electron reactions, the use of a catalyst having a single active site would achieve better results.[22] They hypothesized that the first step in the water redox half reaction is that the bonding between H^+ and catalyst leads to the formation of intermediates. In the second step, the H_2 was released by the combination of either two intermediates, or an intermediate with an H^+ and electrons. Therefore, the two electrons generated in the semiconductor must be transferred to the same metal domain in order for the second step proceeding smoothly (Figure 6A). To verify this hypothesis, CdS nanorods with asymmetrically embedded CdSe quantum dots were prepared, and Pt nanoparticle was grown onto CdS nanorods to form hybrid structures with single, double or multiple reduction sites, respectively. Figure 6B shows that hybrid nanorods with a single metal decoration achieve the best quantum efficiency (QE). The release of H_2 associated with the absorption of two photons for a photocatalyst occurs on a single reduction site. Due to the influence of the Coulomb repulsion, the electrons tend to flow to different active sites when photocatalysts possess more than one reduction locations. In such a case, the intermediate must wait for another photon to be absorbed to the same

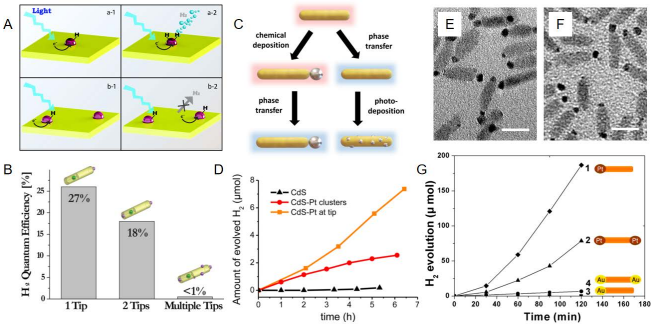

Figure 6 A) Schemes of the formation of hydrogen on a single (a), double (b) metal catalyst. B) Photocatalytic hydrogen evolution quantum efficiency of Pt-CdSe@CdS hybrids with single, double, or multiple tips. C) Scheme of the metal domain decoration and its phase transfer to water. The red and blue background represents the organic and aqueous environment, respectively. D) Photocatalytic hydrogen generation in neutral aqueous solution containing sulfite ions by using Pt-CdSe@CdS hybrids with zero, single or multiple tips. E—F) TEM images of E) single, and F) double Pt-CdSe hybrids, the scale bar is 10 nm. G) Time course of hydrogen generation in a 0.35 M Na_2SO_3/0.25 M Na_2S aqueous solution by using Pt-CdSe and Au-CdSe hybrids with single or double tips. A-B) Reproduced with permission.[22] Copyright 2015, American Chemical Society. C-D) Reproduced with permission.[23] Copyright 2016, American Chemical Society. E-G) Reproduced with permission.[24] Copyright 2012, American Chemical Society.

position to complete the reaction, prolonging the reaction time and decreasing the reaction rate.[22] Figure 6C illustrates two types of metal-CdS hybrid nanorods, one with Pt grown at one end and the other was randomly decorated with multiple Pt clusters.[23] Good contact between the nanorods and Pt particles ensures the possible transfer of the photoexcited electron to the metal domain. Since the distance from the exciton to the Pt domain is much shorter in a multiple-Pt-cluster sample, the electron transfer rate and efficiency are also significantly increased than Pt-tip sample. However, the structure of randomly decorated nanorods shows worse hydrogen production effect than that of the tip decorated structure. They believe that although the speed at which photoexcited electrons transfer to the metal domain increased in the multiple-Pt-cluster sample, it does not guarantee an increase in the amount of electrons involved in the water redox half reaction. In fact, this shortened distance leads to faster charge recombination, which exceeds the advantageous impact of faster electron transfer. It can also be noted in Figure 6D that the catalytic efficiency of samples adorned by multiple Pt clusters gradually decreases over time, possibly due to photooxidation of the hole. This work clearly shows that fewer metal domains with diminishing electron-hole recombination are beneficial in achieving high photocatalytic performance in hydrogen production. Bang *et al.* attributed the different effects of loading metals at different locations to the geometric effect of the metal on the nanorods.[24] Figures 6E and F show that CdSe nanocrystals with a single Pt-tip and double Pt-tips (dumbbell shape) are formed on heterogeneous surface through defect-mediated growth, respectively. The average size of the Pt particles in these two hybrid structures is almost the same. In the single Pt-tipped structure, the CdSe nanorod on the other end which has more activity is in direct contact with the solution, which could facilitates the hole transfer and removal by scavenger after electron transfer to the Pt-tip. In reverse, the holes left can only be transferred and neutralized by the scavenger through the less active, strongly surfactant passivated and defect-free side facets of the dumbbell shape structure which was decorated by Pt nanoparticles on both tips, thus decreasing the charge separation efficiency (Figure 6G).[24]

3.4. Length of nanorods with respect to the core

In metal-semiconductor hybrid nanostructured photocatalysts, the metal domain promotes charge separation of excitons, causing electrons to migrate to the metal domain and then participate in the water splitting half reaction. However, because the recombination of electrons and holes may outweigh the advantages of the metal domain, this promotion of charge separation is not necessarily effective. Therefore, the change in the nanorod lengths, as an influential parameter, will lead to different distances between exciton and reduction site, which will consequently affect the photocatalytic efficiency of hybrid nanostructures.[23,25]

Amirav *et al.* decorated the same size Pt nanoparticles on one of the two end of CdS nanorods embedded with CdSe seeds (Figure 7A) to prepare spatially controlled nano-heterostructures with different lengths of CdSe@CdS nanorods, the relation between nanorod length and their catalytic performance is studied here. The results show that the increase in the length of the CdSe@CdS nanorods provides a higher activity for the same CdSe seed size, resulting in a greatly increased hydrogen production capacity (Figures 7B and 7C). In addition, it was found that the hydrogen generation rate is linear with the light intensity (Figure 7D). This finding indicates that the intermediate of the reduction reaction is stable in this system. Therefore, the physical separation of the reaction sites by elongating the nanorod length appears to be beneficial to the hydrogen generation from photocatalysis.[25b] However, blindly increasing the length of nanorods may suppress electrons transferring to metal part and increase the probability of electron hole recombination, the length matter still needs to be investigated further.

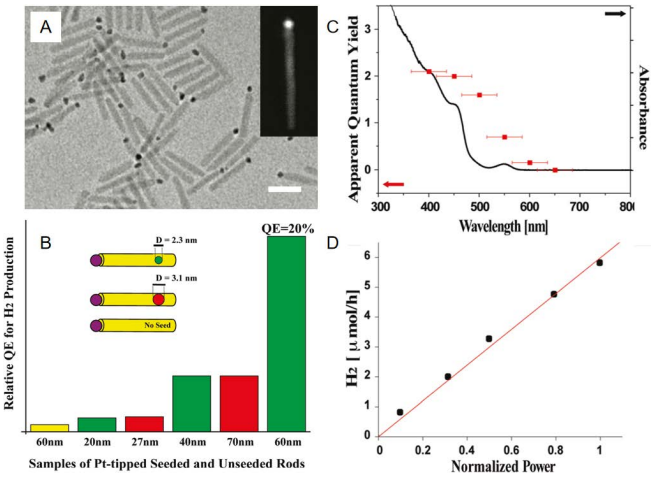

Figure 7 A) TEM images of Pt decorated and CdSe seeded CdS nanorods (average length ≈ 27 nm). The inset is the STEM image of Pt tip, the scale bar is 20 nm. B) Photocatalytic hydrogen production quantum efficiency of Pt-tipped unseeded CdS hybrids (yellow) and seed diameters of 3.1 (red) or 2.3 nm (green) Pt-tipped seeded CdS hybrids. The sizes underneath are the corresponding average length of sample. C) Effect of incident light wavelength on apparent quantum yield of hydrogen production. (D) Effect of the light intensity (white light, 0—1.3 W) on the hydrogen generation rate. A—D) Reproduced with permission.[25a] Copyright 2010, American Chemical Society.

3.5. Solution-liquid-solid method

In a typical metal tipped semiconductor heterostrucutre used for hydrogen production reaction, the reduction reaction will occur in the metal domain while the hole scavenger needs to be introduced to remove OH^- left in the semiconductor domain, otherwise the catalyst will be damaged because lattice sulfide or the surface ligands for passivating with thiol functional group might be oxidized, and charge transfer will be slow down as the recombination of electron and hole might also happen. To bi-functionalized catalyst for effective redox reaction to get both hydrogen and oxygen at the same time, the co-catalysts are involved into this system.[26]

Figure 8A shows a schematic diagram of a photocatalyst with co-catalyst.[26a] Wolff *et al.* synthesized Pt-tipped CdS nanorods and employed a ruthenium complex (a derivative of Ru (tpy)(bpy)Cl_2) anchored on the surface of CdS nanorods as an oxidation catalyst to further improve the efficiency of hole and electron separation and hole transport for subsequent water reduction and oxidation reactions, respectively. The photocatalytic hydrogen evolution rate of CdS nanorods with or without supported oxidation catalyst was tested. In the CdS-Pt system, triethanolamine (TEOA) is used as the hole scavenger and the decoration of Pt and use of TEOA obviously improve the charge separation rate thus showing excellent hydrogen evolution performance (Figures 8B and 8C). When hybrid nanorods are decorated with the oxidation catalyst of RuDTC, the formation rate of hydrogen is only reduced by 25% compared with the CdS-Pt with hole scavengers. This suggests that the oxidation catalyst effectively removes holes throughout the system, and the rate of oxygen generation increases with the number of oxidation catalyst molecules anchored to the nanorods. The characterization results showed that the introduction of oxidation catalyst caused the transfer of ultra-fast hole to RuDTC in 300 fs, which is three orders of magnitude faster than the transfer into hole scavenger. Even though the amount of oxygen generated is smaller than the stoichiometric ratio towards hydrogen evolution, this means there are a small number of holes that may not be able to be removed from the system and the degradation rate of catalysts is significantly diminished, thus

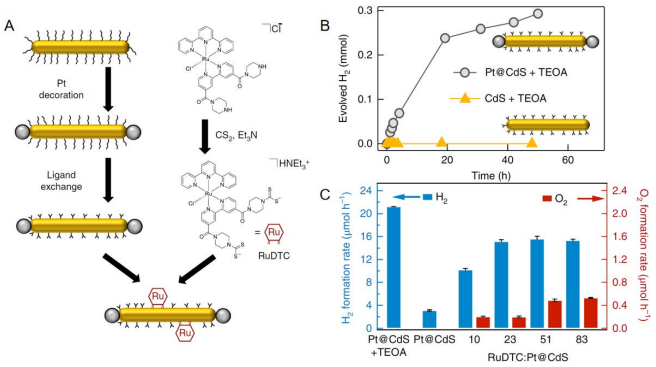

Figure 8 A) Scheme of synthesis method for Pt-CdS hybrids (yellow) by synthesis in organic media, selective growth of Pt nanoparticles (grey) at the tips, and phase transfer into aqueous medium with cysteine and anchoring of the RuDTC catalyst to the side surfaces of the nanorods. B) Hydrogen evolution by bare and tip-decorated CdS nanorods. C) Comparison of average H_2 and O_2 generation rates over the first hour of illumination calculated from at least two measurements for each system. Error bars represent s.d. of measured rates. Sacrificial agent (TEOA) was used only in the first experiment (leftmost blue bar). A—C) Reproduced with permission.[26a] Copyright 2018, Springer Nature.

demonstrating the superiority of the co-catalysts.[26a]

3.6. Band gap structure

In the metal-semiconductor heterostructures, a photocatalyst with excellent performance can be designed by the regulation strategy of the energy band engineering. This is because the maximized synergistic effect can be reached by blending the appropriate components to enhance its catalytic effect.[27]

Zhuang *et al.* constructed a unique 1D binary [ZnS-CdS]-ZnS-[ZnS-CdS]-ZnS structure, a hetero-structure nanorod with multi-nodal sheath CdS, which can achieve better absorbance and charge transport continuity and provide a smaller band gap semiconductor - CdS node sheath.[28] Through selective growth of the metal on the node sheath, the structure of ternary hybrid [ZnS-(CdS/M)]-ZnS-[ZnS-(CdS/M)]-ZnS is obtained. This unique structure enables the transfer of photoexcited electrons from the node sheath of CdS to the metal surface and the ZnS nanorod, and thus can improve the charge separation efficiency. Research on the band gap alignment of materials shows that the binary multi-node sheath nanostructures can be regarded as the connection between ZnS(111) nanorods and ZnS($\bar{1}10$)/CdS($\bar{1}10$) hybrid nodal sheath, and the energy gap of ZnS($\bar{1}10$)/CdS($\bar{1}10$) is located within ZnS(111). Therefore, the binary structure forms a periodic straddling gap alignment (type I heterojunction) (Figure 9B), but there might be an accumulation of electrons and holes in CdS. Therefore, the ternary multi-node sheath with metal loaded nanostructures is investigated then. The calculated workfunction of CdS($\bar{1}10$) is larger than the ($\bar{1}10$) surface of Au, Pd and Pt, so the difference of Fermi energy level/workfunction propels free electrons from Au, Pd or Pt to CdS($\bar{1}10$), thereby bending the CdS band so that it can be staggered with ZnS($\bar{1}10$) and ZnS(111), forming type II heterojunction (Figure 9C). Thus, photogenerated electrons will be transferred to both the metal domain and ZnS-(111). In addition, this structure can also highly suppress the recombination between photoexcitation electron and hole. Tests on the catalytic effect show that the ternary multi-node sheath nanostructures have the highest hydrogen production rate than other structure (Figure 9A), and the best effect is achieved when Pt replaces Au in the ternary structure, which is consistent with the excellent performance of the Pt decorated hybrid nanostructures described in section 3.1.[28]

Ye *et al.* studied the photocatalytic effect of an alloyed semiconductor of ZnS-$CuInS_2$ (ZCIS).[29a] Actually, the band gap energies of $CuInS_2$ (CIS) and ZnS are 1.5 eV and 3.7 eV, respectively, which are not suitable for visible light induced photocatalysis to generate hydrogen from water splitting. However, previous studies by Ye *et al.* have shown that the band gap of ZCIS is highly correlated with alloy composition,[29b] so it is possible to regulate the band gap by alloying, and adjust the ratio of CIS to ZnS to absorb visible light. Compared with the absorption spectrum of CIS, a blue shift occurred for ZCIS, indicating the widen of band gap by introduction of ZnS (Figure 9D). The ZCIS band gap measured was 2.23 eV, which was between the band gap of ZnS and CIS. Based on this, Pt and Pd_4S were decorated on ZCIS to form hybrid nanorods nanostructures, and their photocatalytic properties were tested with Na_2S and Na_2SO_3 as hole scavengers, as shown in Figure 9E. ZCIS-Pt and ZCIS-Pd_4S hybrid nanorods nanostructures showed better photocatalytic performance than naked ZCIS nanorods. This indicates that by constructing heterogeneous structures to regulate the band gap, the materials may possess unprecedented properties that are not available previously, which expands the selection of photocatalyst materials. Compared with traditional photocatalytic materials, it is more feasible to prepare and control heterogeneous catalysts with excellent performance, low price and environmental friendliness.[29a]

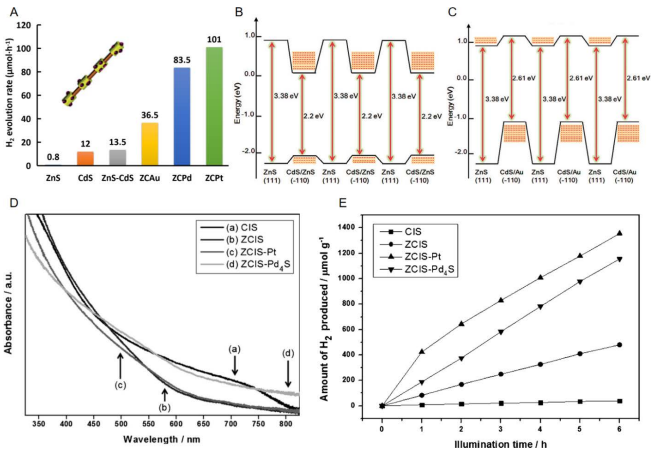

Figure 9 A) Comparison of H_2 evolution rates under visible-light irradiation using different photocatalysts: ZnS nanorods, CdS nanorods, binary ZnS-CdS hetero-nanorods, ternary ZnS-(CdS/Au) hetero-nanorods(ZCAu), ternary ZnS-(CdS/Pd) hetero-nanorods(ZCPd), ternary ZnS-(CdS/Pt) hetero-nanorods(ZCPt). The inset is the representative geometric model of ternary hetero-nanorods with four CdS node sheaths. B) The energy-band alignment of a ZnS(111) nanorod attached by the ZnS($\bar{1}10$)/CdS($\bar{1}10$) hybrid in the periodic binary heterojunction. C) The energy-band alignment of the periodic ternary heterojunction with CdS($\bar{1}10$)/Au hybrids attached to a ZnS(111) nanorod. D) Absorption spectra of the as-prepared samples. a) CIS nanorods, b) ZCIS nanorods, c) ZCIS–Pt hybrid nanorods, and d) ZCIS–Pd_4S hybrid nanorods. E) Photocatalytic hydrogen production under visible-light illumination by CIS nanorods, ZCIS nanorods, ZCIS–Pt hybrid nanorods, and ZCIS–Pd_4S hybrid nanorods from an aqueous solution containing 0.25 M Na_2SO_3 and 0.35 M Na_2S. Measurements were taken every hour for 6 h. A—C) Reproduced with permission.[28] Copyright 2015, Wiley-VCH. D—E) Reproduced with permission.[29a] Copyright 2015, Wiley-VCH.

3.7. Surface ligands

Surface ligand plays an important role in the construction of catalysts. It is used to provide colloidal stability to the photocatalyst in water while maintaining good ability to be close to the active surface to transfer photo-generated excitons. In addition, the passivation of surface defect achieved by coating the ligands can also eliminate trap state thus increasing the photocatalytic properties.

Ben-Shahar and co-workers prepared CdS-Au and CdSe/CdS hybrid nanorods, respectively, with thiolated-alkyl ligands and

polymer coating to study the influence of surface ligands on the catalytic performances. Firstly, hydrophobic phosphonic acid and alkylamine ligands were exchanged to different types of thiolated alkyl ligands, including mercaptocarboxylic acids of different chain lengths (mercaptoundecanoic acid (MUA), mercaptohexanoic acid (MHA) and mercaptopropionic acid (MPA), *L*-glutathione (GSH)) and thiol bound ligands (mercaptosulfonic acid (MSA) and *O*-(2-carboxyethyl)-*O*'-(2-mercaptoethyl) heptaethylene glycol (S-PEG)). Another type is polymer encapsulation, which generally uses polyethylenimine (PEI). PEI binds to the surface of nanorods with amine groups through ligand exchange, and poly(styrene-*co*-maleic anhydride) (PSMA), which can encapsulate the hybrid nanorods to maintain the surface coating of the original nanorods with a hydrophilic end toward the solution. CdS-Au catalysts with different surface coatings were used for photocatalysis. The results of hydrogen production rate and QE are shown in Figures 10A, 10B. Thiolated-alkyl ligands show very low hydrogen production rates, while polymer-coated hetero-structures offer quite high rates, with the hydrogen production rates of PEI coated hybrid nanorods being even an order of magnitude higher than that of MUA coated hetero-structures. In addition, the fastest charge transfer kinetics and particle passivation, and the longer effective fluorescence lifetime of surface ligands can be obtained with PEI coating. Stone and colleagues used a similar surface encapsulation strategy in which the PEI coated nanocrystals achieved excellent catalytic performance than thiolated alkyl ligands.[11] Through the passivation of surface defects and decreasing of available hole trapping sites, the effective charge transfer across the semiconductor-metal interface can be realized.[30]

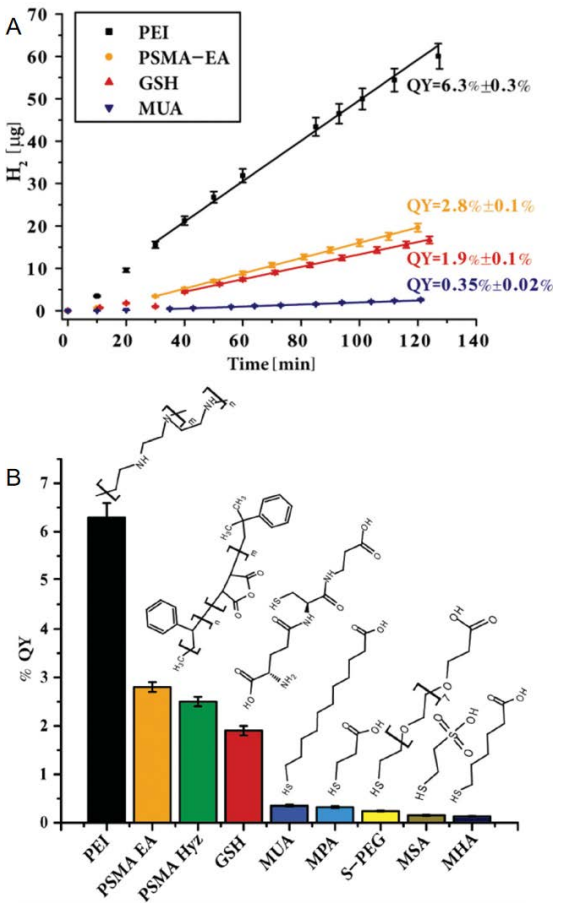

Figure 10 A) Kinetic hydrogen evolution measurements by CdS-Au hybrid nanorods for different surface coatings. Straight lines represent the linear fits from which the %QY was extracted. B) Apparent photocatalysis %QY values for a wide range of surface coatings including thiolated alkyl ligands, GSH, and polymer coating. PEI exhibits the highest QY. A—B) Reproduced with permission.[30] Copyright 2014, Wiley-VCH.

3.8. Hole scavenger

It is well known that electrons and holes are generated when semiconductor nanorods are irradiated with sunlight. The photo-excited electrons are transferred to the metal domain to reduce water to hydrogen, while the photogenerated holes require the addition of scavenger to remove. The introduction of hole scavenger not only suppresses electron-hole recombination but also prevents photo-corrosion of the metal sulfide semiconductor. Therefore, the addition of sacrificial agent is very important in photocatalytic reaction. In addition, different hole scavenger will bring different degrees of influence and improper scavenger may even reduce the performance of the catalyst.[31]

Wu *et al.* used MUA-capped CdSe/CdS-Pt and CdS-Pt hybrid nanorods to study the performance of methanol (MeOH) and sulfite as hole scavengers for photocatalytic hydrogen generation (Figures 11A and B). Both CdSe/CdS-Pt and CdS-Pt nanorods have achieved efficient charge separation and long-life charge separation states, the hole transfer rate is positively correlated with hydrogen generation QE. Combining the characterization results and calculation data, the use of MeOH scavenger on CdS-Pt nanocrystals exhibits the lowest rate in the hole transferring. The hole transfer rate from CdSe/CdS-Pt to the MUA and MeOH is about 4.9 times faster than that of CdS-Pt. The combination of MUA and highly reductive sulfites provides a greater driving force for hole removal, making the effect of this group better than the group using MeOH as an electron donor. The interaction of the hole acceptor with the surface-capping ligand, the accessibility of the surface sites, and the strong reducibility of the sulfite cause more holes in the surface trap of the CdS-Pt nanorod to be removed, which is reflected in the fact that the hole transfer time from CdS-Pt to sulfite is about 2.5 times faster than that of CdSe/CdS-Pt.[32] In addition, Berr *et al.* also studied the catalytic performances of four hole scavengers for Pt-CdS nanorods such as sodium sulfite (SO_3^{2-}), disodium ethylenediaminetetraacetic acid

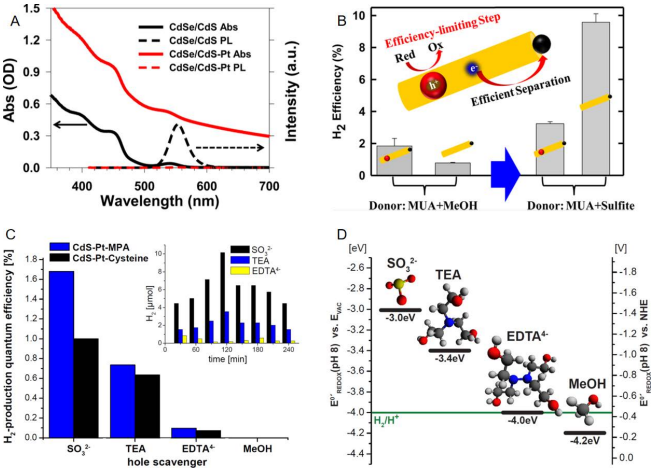

Figure 11 A) Static absorption (solid lines) and photoluminescence (PL, dashed lines) spectra of CdSe/CdS NRs (black lines) and CdSe/CdSPt nanorods (red lines). B) Steady state photocatalytic hydrogen evolution QYs using MUA-capped CdSe/CdS-Pt and CdS-Pt nanorods, with either methanol or sodium sulfite as additional sacrificial electron donors. The inset shows the CdSe seeded CdS nanorod with Pt tip. C) Comparison of quantum efficiencies for Pt-decorated CdS nanorods using SO_3^{2-}, TEA, $EDTA^{4-}$, and MeOH as hole scavengers. Data for different ligands (*i.e.*, MPA and cysteine) are shown. The inset shows the hydrogen evolution as a function of time for MPA-stabilized nanorods and different hole scavengers. D) Schematic plot of the energy levels of the electrons of hole scavengers that are involved in the reduction of the photohole vs. vacuum and on normal hydrogen electrode (NHE) scale. A—B) Reproduced with permission.[32] Copyright 2014, American Chemical Society. C—D) Reproduced with permission.[33] Copyright 2012, American Institute of Physics.

($EDTA^{4-}$), triethanolamine (TEA) and MeOH, respectively.[33] As can be seen from Figure 11C, SO_3^{2-} achieves the best results with a QE that can exceed an order of magnitude of the worst one such as MeOH. They believe that this is the result of different redox potentials of hole scavengers. As shown in Figure 11D, SO_3^{2-} has the strongest reducibility and is more easily oxidized by the combination of holes. Besides, the morphology of the catalyst after photocatalysis using different hole scavengers indicates that the nanorods using MeOH as hole scavenger are shortened and aggregated while the nanorods using SO_3^{2-} can remain their morphology after catalysis because the electron donor timely cleared the holes captured by the surface traps of the nanorods, which prevented the photooxidation of catalyst.[33]

3.9. Other strategies nanorods

In addition to the widely studied 1D colloidal metal-semiconductor nanorod heterostructures and the aforementioned engineering strategies, there are many other systems and strategies to improve photocatalytic hydrogen production efficiency. Most of them follow the same principle, *i.e.*, to achieve better charge separation.[1f,34] Zhang *et al.* conducted amine-assisted directional growth of CdS nanords with MoS_2 tips (M-t-CdS) (Figure 12A).

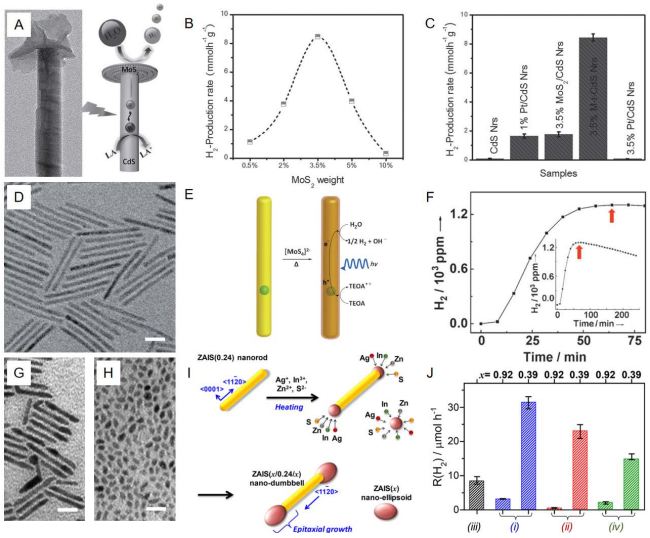

Figure 12 A) Schematic representation of photocatalytic H_2 generation on MoS_2-CdS nanorods. B) H_2 evolution rates of MoS_2-CdS nanorods with different MoS_2 content. C) Comparison of H_2 evolution rates between CdS nanorods, 1 wt% Pt/CdS nanorods, 3.5 wt% MoS_2/CdS nanorods, 3.5 wt% MoS_2-CdS nanorods, and 3.5% Pt/CdS nanorods. D) Bright-field TEM image of CdSe-seeded CdS nanorods (length 60 nm). E) MoS_3 deposition on a CdSe-seeded CdS nanorod, with photocatalytic hydrogen production in the visible range using triethanolamine (TEOA) as a sacrificial reductant. F) A typical gas chromatogram observed for a MoS_3-coated CdS/CdSe nanorod using 450 nm light with an induction period of approximately 50 min. 0.07 nmol of rods were used with 5.0 mL 0.1 M tris buffer (pH 7.0) and 0.20 mL TEOA. The inset shows the measurement over a period of 4 h. The activities are derived from the maximum rate of H_2 produced, as indicated by the arrows. G—H) Wide-area TEM images of ZAIS nanodumbbells prepared when x_p = 0.5 and corresponding ZAIS nanoellipsoids simultaneously formed as a byproduct. ZAIS nanocrystals of each shape were separated from as-prepared mixture nanocrystals by a size-selective precipitation technique. I) Schematic illustration of the formation mechanism of ZAIS nanodumbbells and nanoellipsoids. J) Dependence of $R(H_2)$ on the kind of ZAIS nanocrystals used. Samples were (i) ZAIS(x/0.24/x) nanodumbbells, (ii) ZAIS(x) nanoellipsoids, (iii) ZAIS(0.24) nanorods, and (iv) mixtures of ZAIS(0.24) nanorods and ZAIS(x) nanoellipsoids (1 : 2). The scale bar is 20 nm. A—C) Reproduced with permission.[35] Copyright 2016, Wiley-VCH. D—F) Reproduced with permission.[36] Copyright 2011, Wiley-VCH. G—J) Reproduced with permission.[37] Copyright 2018, American Chemical Society.

Results show that the photocatalytic activity of the M-t-CdS heterostructure containing 3.5 wt% of MoS_2 is optimal. The PL emission of the M-t-CdS nanorods trap states is also significantly reduced which indicates their longer lifetime (photocatalytic hydrogen production can be carried out for more than 23 h). The M-t-CdS heterostructure provides a large contact area between CdS nanorods and hole scavengers, thus hindering recombination of photoelectron and hole to achieve efficient carrier separation (Figures 12B and 12C).[35] Besides, the coating of amorphous MoS_3 surface on semiconductor nanorods was studied by Tang *et al.* who used $(NH_4)_2MoS_4$ with one-step heat treatment to deposit amorphous MoS_3 film on CdSe/CdS nanorods (Figures 12D and 12E). The close contact between the MoS_3 surface layer and the nanorods enhances charge transfer. The system is highly active and can efficiently produce photocatalytic hydrogen. A drawback of this system is that the surface coating is relatively easy to dissolve, even in the absence of light. This thereby reduces the rate of hydrogen generation over time (Figure 12F).[36]

Kameyama *et al.* studied a special nanocrystals heterostructure of ZnS-$AgInS_2$ solid solution ($(AgIn)_xZn_{2(1-x)}S_2$, ZAIS). The dumbbell-shaped Zn-Ag-In-S nanocrystals with adjustable photocatalytic activity were prepared by growing ZAIS nanocrystals at both ends of ZAIS nanorod (the composition of the rods is $(AgIn)_{0.24}Zn_{1.52}S_2$). By regulating the x value of ZAIS nano-ellipsoid $(AgIn)_xZn_{2(1-x)}S_2$ (Figures 12G—I), the optimal combination was sought. Since the conduction band and valence band edge energy levels of ZAIS nanocrystals are regulated by shape, size and composition, they can be used to design the band alignment of ZAIS nanocrystal heterojunctions, which will greatly improve the photocatalytic performance of ZAIS nanocrystals (Figure 12J).[37]

In conclusion, the engineering strategies of 1D metal-semiconductor hybrid nanorods are summarized in this section, the photocatalysis performance of hydrogen generation from water splitting can be boosted through these engineering strategies. Apart from that, these elegant 1D hybrid nanostructures with enhanced electronic property and charge separation ability can also be utilized in many fields, such as CO_2 reduction,[38] photoelectrochemical cell,[39] sensor,[40] photodynamic therapy,[41] *etc.* These 1D hybrid structures have broad application prospects and further research in this field is highly demanded.

4. Conclusion and Outlook

This review presents a variety of strategies to engineer the metal-semiconductor nanorods hybrid nanostructures so that their electronic properties could be tuned to perform optimal photocatalytic functions in solar-driven water splitting. While the scope of this engineering is broad and the photocatalytic properties of derived hybrid nanomaterials are impressive, this area of research still faces significant challenges before the full potential of the hybrid nanomaterials is realized. One challenge is to expand these engineering strategies from cadmium-based 1D hybrid structures to additional semiconductor materials, in particular to heavy-metal-free systems. Non-precious metal decorated III-V semiconductors would be competitive candidates in this aspect but research on this is still in its infancy. This will require further development of synthetic routes in combination with emerging engineering strategies which may lead to less or even non-toxic "green" photocatalysts for solar-driven fuel production through water splitting but also may provide an avenue to sustainable and environmentally friendly clean fuels. On the other hand, most studies relating to the hybrid nanorods were mainly focusing on hydrogen evolution reaction and used the hole scavenger as electron donor. The construction of multifunctional heterostructure seems to be a promising approach to enhance hydrogen evolution reaction. For example, the hybrid nanorod decorated with Ru can serve as the photooxidation co-catalyst which can prevent the catalysts from degradation induced by holes accumulation and

can achieve efficient overall water splitting.

Chemical corrosion and photodegradation are the main problems of these 1D metal-semiconductor hybrid catalysts. The adoption of organic ligand coatings to passivate surface defects and the use of hole scavenger to remove photo-generated holes can be used to effectively improve the stability of 1D metal-semiconductor heterostructures. The use of other materials (such as amorphous TiO_2) as coatings is also an effective way to protect the hybrid structure and achieve multifunctionality. More research is demanded to solve this problem to realize the practical application of these hybrid nanorods in photocatalytic hydrogen evolution from water splitting.

It is worth noting that this review is mainly focused on metal-semiconductor nanorods hybrid nanostructures with elongated shape. Two-dimensional (2D) metal-semiconductor nanoplatelets hybrid nanostructures with excitons being confined in their thickness direction are less studies and not well developed. As the catalytic reactions are more likely to take place on the edge atoms, selectively depositing the metal atoms, especially the noble metal atoms, onto the edges of semiconductor nanoplatelets will increase their exposure, which can reduce their amount of deposition and cost. Furthermore, exploration of the engineering strategies to this type of intriguing hybrid materials is meaningful and exciting because studies into this area may lead to unexpected observations and unprecedented photocatalytic performances.

To summarize, metal-semiconductor hybrid nanoparticles have significant potential in solar-driven photocatalysis for clean fuel production. The remarkable advances in the engineering strategies of these materials alongside with the in-depth understanding the physico-chemical principals that govern the photocatalytic reactions provide a solid basis for their photocatalytic applications.

Acknowledgement

This work is supported by the Australian Research Council (ARC) Future Fellowship Scheme (FT210100509), ARC Discovery Project (DP220101959), the Hebrew University of Jerusalem - Zelman Cowen Academic Initiatives (ZCAI) Joint Projects 2021, the Innovation and Technology Commission (grant no. MHP/104/21), Shenzhen Science Technology and Innovation Commission (grant no. 20210324125612035), and City University of Hong Kong (grant no. 9360140).

References

[1] (a) Wang, T.; Zhuang, J.; Lynch, J.; Chen, O.; Wang, Z.; Wang, X.; LaMontagne, D.; Wu, H.; Wang, Z.; Cao, Y. C. Self-Assembled Colloidal Superparticles from Nanorods. *Science* **2012**, *338*, 358–363; (b) Hu, J.; Li, L. S.; Yang, W.; Manna, L.; Wang, L. W.; Alivisatos, A. P. Linearly Polarized Emission from Colloidal Semiconductor Quantum Rods. *Science* **2001**, *292*, 2060–2063; (c) Wolff, C. M.; Frischmann, P. D.; Schulze, M.; Bohn, B. J.; Wein, R.; Livadas, P.; Carlson, M. T.; Jäckel, F.; Feldmann, J.; Würthner, F.; Stolarczyk, J. K. All-in-One Visible-Light-Driven Water Splitting by Combining Nanoparticulate and Molecular Co-catalysts on CdS Nanorods. *Nat. Energy* **2018**, *3*, 862–869; (d) Pawar, A. A.; Halivni, S.; Waiskopf, N.; Ben-Shahar, Y.; Soreni-Harari, M.; Bergbreiter, S.; Banin, U.; Magdassi, S. Rapid Three-Dimensional Printing in Water Using Semiconductor–Metal Hybrid Nanoparticles as Photoinitiators. *Nano Lett.* **2017**, *17*, 4497–4501; (e) Chen, D.; Zhang, H.; Li, Y.; Pang, Y.; Yin, Z.; Sun, H.; Zhang, L. C.; Wang, S.; Saunders, M.; Barker, E.; Jia, G. Spontaneous Formation of Noble–and Heavy–Metal–Free Alloyed Semiconductor Quantum Rods for Efficient Photocatalysis. *Adv. Mater.* **2018**, *30*, 1803351; (f) Jia, G.; Pang, Y.; Ning, J.; Banin, U.; Ji, B. Heavy–Metal–Free Colloidal Semiconductor Nanorods: Recent Advances and Future Perspectives. *Adv. Mater.* **2019**, *31*, 1900781; (g) Huynh, W. U.; Dittmer, J. J.; Alivisatos, A. P. Hybrid Nanorod-Polymer Solar Cells. *Science* **2002**, *295*, 2425–2427; (h) Jia, G.; Sitt, A.; Hitin, G. B.; Hadar, I.; Bekenstein, Y.; Amit, Y.; Popov, I.; Banin, U. Couples of Colloidal Semiconductor Nanorods Formed by Self-Limited Assembly. *Nat. Mater.* **2014**, *13*, 301–307; (i) Jia, G.; Banin, U. A General Strategy for Synthesizing Colloidal Semiconductor Zinc Chalcogenide Quantum Rods. *J. Am. Chem. Soc.* **2014**, *136*, 11121–11127.

[2] (a) Waiskopf, N.; Ben-Shahar, Y.; Banin, U. Photocatalytic Hybrid Semiconductor–Metal Nanoparticles; from Synergistic Properties to Emerging Applications. *Adv. Mater.* **2018**, *30*, 1706697; (b) Lo, S. S.; Mirkovic, T.; Chuang, C.; Burda, C.; Scholes, G. D. Emergent Properties Resulting from Type-II Band Alignment in Semiconductor Nanoheterostructures. *Adv. Mater.* **2011**, *23*, 180–197; (c) Tan, C.; Chen, J.; Wu, X.; Zhang, H. Epitaxial Growth of Hybrid Nanostructures. *Nat. Rev. Mater*. **2018**, *3*, 17089; (d) Wu, K.; Chen, J.; McBride, J. R.; Lian, T. Efficient Hot-Electron Transfer by a Plasmon-Induced Interfacial Charge-Transfer Transition. *Science* **2015**, *349*, 632–635.

[3] (a) Oh, N.; Kim, B. H.; Cho, S. Y.; Nam, S.; Rogers, S. P.; Jiang, Y.; Flanagan, J. C.; Zhai, Y.; Kim, J. H.; Lee, J.; Yu, Y.; Cho, Y. K.; Hur, G.; Zhang, J.; Trefonas, P.; Rogers, J. A.; Shim, M. Double-Heterojunction Nanorod Light-Responsive LEDs for Display Applications. *Science* **2017**, *355*, 616–619; (b) Kumar, S.; Jones, M.; Lo, S. S.; Scholes, G. D. Nanorod Heterostructures Showing Photoinduced Charge Separation. *Small* **2007**, *3*, 1633–1639; (c) Vaneski, A.; Susha, A. S.; Rodríguez-Fernández, J.; Berr, M.; Jäckel, F.; Feldmann, J.; Rogach, A. L. Hybrid Colloidal Heterostructures of Anisotropic Semiconductor Nanocrystals Decorated with Noble Metals: Synthesis and Function. *Adv. Funct. Mater.* **2011**, *21*, 1547–1556; (d) Tada, H.; Mitsui, T.; Kiyonaga, T.; Akita, T.; Tanaka, K. All-Solid-State Z-Scheme in CdS–Au–TiO_2 Three-Component Nanojunction System. *Nat. Mater.* **2006**, *5*, 782–786; (e) Maynadie, J.; Salant, A.; Falqui, A.; Respaud, M.; Shahiv, E.; Banin, U.; Soulantica, K.; Chaudret, B. Cobalt Growth on the Tips of CdSe Nanorods. *Angew. Chem. Int. Ed.* **2009**, *48*, 1814–1817.

[4] (a) Zhong, D. K.; Sun, J.; Inumaru, H.; Gamelin, D. R. Solar Water Oxidation by Composite Catalyst/α-Fe_2O_3 Photoanodes. *J. Am. Chem. Soc.* **2009**, *131*, 6086–6087; (b) Dotan, H.; Mathews, N.; Hisatomi, T.; Gratzel, M.; Rothschild, A. On the Solar to Hydrogen Conversion Efficiency of Photoelectrodes for Water Splitting. *J. Phys. Chem. Lett.* **2014**, *5*, 3330–3334; (c) Dutta, S. K.; Mehetor, S. K.; Pradhan, N. Metal Semiconductor Heterostructures for Photocatalytic Conversion of Light Energy. *J. Phys. Chem. Lett.* **2015**, *6*, 936–944; (d) Simon, T.; Bouchonville, N.; Berr, M. J.; Vaneski, A.; Adrović, A.; Volbers, D.; Wyrwich, R.; Döblinger, M.; Susha, A. S.; Rogach, A. L.; Jäckel, F.; Stolarczyk, J. K.; Feldmann, J. Redox Shuttle Mechanism Enhances Photocatalytic H_2 Generation on Ni-Decorated CdS Nanorods. *Nat. Mater.* **2014**, *13*, 1013–1018.

[5] (a) Cozzoli, P. D.; Pellegrino, T.; Manna, L. Synthesis, Properties and Perspectives of Hybrid Nanocrystal Structures. *Chem. Soc. Rev.* **2006**, *35*, 1195–1208; (b) Carbonea, L.; Cozzoli, P. D. Colloidal Heterostructured Nanocrystals: Synthesis and Growth Mechanisms. *Nano Today* **2010**, *5*, 449–493; (c) Banin, U.; Ben-Shahar, Y.; Vinokurov, K. Hybrid Semiconductor–Metal Nanoparticles: From Architecture to Function. *Chem. Mater.* **2014**, *26*, 97–110; (d) Jiang, R.; Li, B.; Fang, C.; Wang, J. Metal/Semiconductor Hybrid Nanostructures for Plasmon-Enhanced Applications. *Adv. Mater.* **2014**, *26*, 5274–5309; (e) Costi, R.; Saunders, A. E.; Banin, U. Colloidal Hybrid Nanostructures: A New Type of Functional Materials. *Angew. Chem. Int. Ed.* **2010**, *49*, 4878–4897.

[6] (a) Demortière, A.; Schaller, R. D.; Li, T.; Chattopadhyay, S.; Krylova, G.; Shibata, T.; Claro, P. C. dos S.; Rowland, C. E.; Miller, J. T.; Cook, R.; Lee, B.; Shevchenko, E. V. In Situ Optical and Structural Studies on Photoluminesence Quenching in CdSe/CdS/Au Heterostructures. *J. Am. Chem. Soc.* **2014**, *136*, 2342–2350; (b) Mokari, T.; Rothenberg, E.; Popov, I.; Costi, R.; Banin, U. Selective Growth of Metal Tips onto Semiconductor Quantum Rods and Tetrapods. *Science* **2004**, *304*, 1787–1790; (c) Dukovic, G.; Merkle, M. G.; Nelson, J. H.; Hughes, S. M.; Alivisatos, A. P. Photodeposition of Pt on Colloidal CdS and CdSe/CdS Semiconductor Nanostructures. *Adv. Mater.* **2008**, *20*, 4306–4311; (d) Menagen, G.; Macdonald, J. E.; Shemesh, Y.; Popov, I.; Banin, U. Au Growth on Semiconductor Nanorods: Photoinduced

versus Thermal Growth Mechanisms. *J. Am. Chem. Soc.* **2009**, *131*, 17406–17411.

[7] Bala, T.; Singh, A.; Sanyal, A.; O'Sullivan, C.; Laffir, F.; Coughlan, C.; Ryan, K. M. Fabrication of Noble Metal-Semiconductor Hybrid Nanostructures Using Phase Transfer. *Nano Res.* **2013**, *6*, 121–130.

[8] (a) Cozzoli, P. D.; Pellegrino, T.; Manna, L. Synthesis, Properties and Perspectives of Hybrid Nanocrystal Structures. *Chem. Soc. Rev.* **2006**, *35*, 1195–1208; (b) Coughlan, C.; Singh, A.; Ryan, K. M. Systematic Study into the Synthesis and Shape Development in Colloidal $CuIn_xGa_{1-x}S_2$ Nanocrystals. *Chem. Mater.* **2013**, *25*, 653–661; (c) Wang, F.; Wang, Y.; Liu, Y.; Morrison, P. J.; Loomis, R. A.; Buhro, W. E. Two-Dimensional Semiconductor Nanocrystals: Properties, Templated Formation, and Magic-Size Nanocluster Intermediates. *Acc. Chem. Res.* **2015**, *48*, 13–21; (d) Wang, F.; Dong, A.; Sun, J.; Tang, R.; Yu, H.; Buhro, W. E. Solution−Liquid−Solid Growth of Semiconductor Nanowires. *Inorg. Chem.* **2006**, *45*, 7511–7521.

[9] Shen, H.; Shang, H.; Niu, J.; Xu, W.; Wang, H.; Li, L. Size– and Shape–Dependent Growth of Fluorescent ZnS Nanorods and Nanowires Using Ag Nanocrystals as Seeds. *Nanoscale* **2012**, *4*, 6509–6514.

[10] (a) Chakrabortty, S.; Xing, G.; Xu, Y.; Ngiam, S. W.; Mishra, N.; Sum, T. C.; Chan, Y. Engineering Fluorescence in Au-Tipped, CdSe-Seeded CdS Nanoheterostructures. *Small* **2011**, *7*, 2847–2852; (b) Kraus-Ophir, S.; Ben-Shahar, Y.; Banin, U.; Mandler, D. Perpendicular Orientation of Anisotropic Au-Tipped CdS Nanorods at the Air/Water Interface. *Adv. Mater. Interfaces* **2014**, *1*, 1300030; (c) Zhao, N.; Vickery, J.; Guerin, G.; Park, J. I.; Winnik, M. A.; Kumacheva, E. Self-Assembly of Single–Tip Metal–Semiconductor Nanorods in Selective Solvents. *Angew. Chem. Int. Ed.* **2011**, *50*, 4606–4610; (d) Rukenstein, P.; Teitelboim, A.; Volokh, M.; Diab, M.; Oron, D.; Mokari, T. Charge Transfer Dynamics in CdS and CdSe@CdS Based Hybrid Nanorods Tipped with Both PbS and Pt. *J. Phys. Chem. C* **2016**, *120*, 15453–15459; (e) Yu, P.; Wen, X.; Lee, Y.; Lee, W.; Kang, C.; Tang, J. Photoinduced Ultrafast Charge Separation in Plexcitonic CdSe/Au and CdSe/Pt Nanorods *J. Phys. Chem. Lett.* **2013**, *4*, 3596–3601; (f) O'Connor, T.; Panov, M. S.; Mereshchenko, A.; Tarnovsky, A. N.; Lorek, R.; Perera, D.; Diederich, G.; Lambright, S.; Moroz, P.; Zamkov, M. The Effect of the Charge-Separating Interface on Exciton Dynamics in Photocatalytic Colloidal Heteronanocrystals. *ACS Nano* **2012**, *6*, 8156–8165; (g) Zeng, D.; Chen, Y.; Wang, Z.; Wang, J.; Xie, Q.; Peng, D. Synthesis of Ni–Au–ZnO Ternary Magnetic Hybrid Nanocrystals with Enhanced Photocatalytic Activity. *Nanoscale* **2015**, *7*, 11371–11378; (h) Ganai, A.; Maiti, P. S.; Houben, L.; Bar-Ziv, R.; Sadan, M. B. Inside-Out: The Role of Buried Interfaces in Hybrid Cu_2ZnSnS_4–Noble Metal Photocatalysts. *J. Phys. Chem. C* **2017**, *121*, 7062–7068; (i) Retamal, J. R. D.; Periyanagounder, D.; Ke, J.; Tsai, M.; He, J. Charge Carrier Injection and Transport Engineering in Two-Dimensional Transition Metal Dichalcogenides. *Chem. Sci.* **2018**, *9*, 7727–7745.

[11] Stone, D.; Ben-Shahar, Y.; Waiskopf, N.; Banin, U. The Metal Type Governs Photocatalytic Reactive Oxygen Species Formation by Semiconductor-Metal Hybrid Nanoparticles. *ChemCatChem* **2018**, *10*, 5119–5123.

[12] Tongying, P.; Vietmeyer, F.; Aleksiuk, D.; Ferraudi, G. J.; Krylova, G.; Kuno, M. Double Heterojunction Nanowire Photocatalysts for Hydrogen Generation. *Nanoscale* **2014**, *6*, 4117–4124.

[13] Aronovitch, E.; Kalisman, P.; Houben, L.; Amirav, L.; Bar-Sadan, M. Stability of Seeded Rod Photocatalysts: Atomic Scale View. *Chem. Mater.* **2016**, *28*, 1546–1552.

[14] (a) Xu, Y.; Ruban, A. V.; Mavrikakis, M. Adsorption and Dissociation of O_2 on Pt−Co and Pt−Fe Alloys. *J. Am. Chem. Soc.* **2004**, *126*, 4717–4725; (b) Tao, F.; Grass, M. E.; Zhang, Y.; Butcher, D. R.; Renzas, J. R.; Liu, Z.; Chung, J. Y.; Mun, B. S.; Salmeron, M.; Somorjai, G. A. Reaction–Driven Restructuring of Rh–Pd and Pt–Pd Core–Shell Nanoparticles. *Science* **2008**, *322*, 932–934.

[15] Kalisman, P.; Houben, L.; Aronovitch, E.; Kauffmann, Y.; Bar-Sadanc, M.; Amirav, L. The Golden Gate to Photocatalytic Hydrogen Production. *J. Mater. Chem. A* **2015**, *3*, 19679–19682.

[16] Maynadié, J.; Salant, A.; Falqui, A.; Respaud, M.; Shaviv, E.; Banin, U.; Soulantica, K.; Chaudret, B. Cobalt Growth on the Tips of CdSe Nanorods. *Angew. Chem. Int. Ed.* **2009**, *48*, 1814–1817.

[17] (a) Schweinberger, F. F.; Berr, M. J.; Döblinger, M.; Wolff, C.; Sanwald, K. E.; Crampton, A. S.; Ridge, C. J.; Jäckel, F.; Feldmann, J.; Tschurl, M.; Heiz, U. Cluster Size Effects in the Photocatalytic Hydrogen Evolution Reaction. *J. Am. Chem. Soc.* **2013**, *135*, 13262–13265; (b) Tian, Y.; Wang, L.; Yu, S.; Zhou, W. Heterostructure of Au Nanocluster Tipping on a ZnS Quantum Rod: Controlled Synthesis and Novel Luminescence. *Nanotechnology* **2015**, *26*, 325702; (c) O'Sullivan, C.; Gunning, R. D.; Barrett, C. A.; Singhab, A.; Ryan, K. M. Size Controlled Gold Tip Growth onto II–VI Nanorods. *J. Mater. Chem.* **2010**, *20*, 7875–7880; (d) Khalavka, Y.; Harms, S.; Henkel, A.; Strozyk, M.; Ahijado-Guzmán, R.; Sönnichsen, C. Synthesis of Au–CdS@CdSe Hybrid Nanoparticles with a Highly Reactive Gold Domain. *Langmuir* **2018**, *34,* 187–190; (e) Waiskopf, N.; Ben-Shahar, Y.; Galchenko, M.; Carmel, I.; Moshitzky, G.; Soreq, H.; Banin, U. Photocatalytic Reactive Oxygen Species Formation by Semiconductor–Metal Hybrid Nanoparticles. Toward Light–Induced Modulation of Biological Processes. *Nano Lett.* **2016**, *16*, 4266–4273.

[18] Ben-Shahar, Y.; Philbin, J. P.; Scotognella, F.; Ganzer, L.; Cerullo, G.; Rabani, E.; Banin, U. Charge Carrier Dynamics in Photocatalytic Hybrid Semiconductor–Metal Nanorods: Crossover from Auger Recombination to Charge Transfer. *Nano Lett.* **2018**, *18*, 5211–5216.

[19] Nakibli, Y.; Mazal, Y.; Dubi, Y.; Wächtler, M.; Amirav, L. Size Matters: Cocatalyst Size Effect on Charge Transfer and Photocatalytic Activity. *Nano Lett.* **2018**, *18*, 357–364.

[20] Ben-Shahar, Y.; Scotognella, F.; Kriegel, I.; Moretti, L.; Cerullo, G.; Rabani, E.; Banin, U. Optimal Metal Domain Size for Photocatalysis with Hybrid Semiconductor–Metal Nanorods. *Nat. Commun.* **2016**, *7*, 10413.

[21] (a) Shaviv, E.; Schubert, O.; Alves-Santos, M.; Goldoni, G.; Felice, R. D.; Vallée, F.; Fatti, N. D.; Banin, U.; Sönnichsen, C. Absorption Properties of Metal–Semiconductor Hybrid Nanoparticles *ACS Nano* **2011**, *5*, 4712–4719; (b) Alemseghed, M. G.; Ruberu, T. P. A.; Vela, J. Controlled Fabrication of Colloidal Semiconductor–Metal Hybrid Heterostructures: Site Selective Metal Photo Deposition *Chem. Mater.* **2011**, *23*, 3571–3579; (c) Caddeo, C.; Calzia, V.; Bagolini, L.; Lusk, M. T.; Mattoni, A. Pinpointing the Cause of Platinum Tipping on CdS Nanorods. *J. Phys. Chem. C* **2015**, *119*, 22663–22668; (d) Schlicke, H.; Ghosh, D.; Fong, L.; Xin, H. L.; Zheng, H.; Alivisatos, A. P. Selective Placement of Faceted Metal Tips on Semiconductor Nanorods. *Angew. Chem. Int. Ed.* **2013**, *52*, 980–982; (e) Hill, L. J.; Bull, M. M.; Sung, Y.; Simmonds, A. G.; Dirlam, P. T.; Richey, N. E.; DeRosa, S. E.; Shim, I.; Guin, D.; Costanzo, P. J.; Pinna, N.; Willinger, M.; Vogel, W.; Char, K.; Pyun, J. Directing the Deposition of Ferromagnetic Cobalt onto Pt–Tipped CdSe@CdS Nanorods: Synthetic and Mechanistic Insights. *ACS Nano* **2012**, *6*, 8632–8645; (f) Ha, J. W.; Ruberu, T. P. A.; Han, R.; Dong, B.; Vela, J.; Fang, N. Super–Resolution Mapping of Photogenerated Electron and Hole Separation in Single Metal–Semiconductor Nanocatalysts. *J. Am. Chem. Soc.* **2014**, *136*, 1398–1408.

[22] Nakibli, Y.; Kalisman, P.; Amirav, L. Less Is More: The Case of Metal Cocatalysts. *J. Phys. Chem. Lett.* **2015**, *6*, 2265–2268.

[23] Simon, T.; Carlson, M. T.; Stolarczyk, J. K.; Feldmann, J. Electron Transfer Rate vs Recombination Losses in Photocatalytic H_2 Generation on Pt–Decorated CdS Nanorods. *ACS Energy Lett.* **2016**, *1*, 1137–1142.

[24] Bang, J. U.; Lee, S. J.; Jang, J. S.; Choi, W.; Song, H. Geometric Effect of Single or Double Metal–Tipped CdSe Nanorods on Photocatalytic H_2 Generation. *J. Phys. Chem. Lett.* **2012**, *3*, 3781–3785.

[25] (a) Amirav, L.; Alivisatos, A. P. Photocatalytic Hydrogen Production with Tunable Nanorod Heterostructures. *J. Phys. Chem. Lett*. **2010**, *1*, 1051–1054; (b) Bridewell, V. L.; Alam, R.; Karwacki, C. J.; Kamat, P. V. CdSe/CdS Nanorod Photocatalysts: Tuning the Interfacial Charge Transfer Process through Shell Length. *Chem. Mater.* **2015**, *27*, 5064–5071.

[26] (a) Wolff, C. M.; Frischmann, P. D.; Schulze, M.; Bohn, B. J.; Wein, R.; Livadas, P.; Carlson, M. T.; Jäckel, F.; Feldmann, J.; Würthner, F.; Stolarczyk, J. K. All–In–One Visible–Light–Driven Water Splitting by Combining Nanoparticulate and Molecular Co–Catalysts on CdS Na-

norods. *Nat. Energy*. **2018**, *3*, 862–869; (b) Kuehnel, M. F.; Creissen, C. E.; Sahm, C. D.; Wielend, D.; Schlosser, A.; Orchard, K. L.; Reisner, E. ZnSe Nanorods as Visible–Light Absorbers for Photocatalytic and Photoelectrochemical H_2 Evolution in Water. *Angew. Chem. Int. Ed*. **2019**, *131*, 5113–5117.

[27] (a) Zhuang, T.; Liu, Y.; Li, Y.; Sun, M.; Sun, Z.; Du, P.; Jiang, J.; Yu, S. 1D Colloidal Hetero–Nanomaterials with Programmed Semiconductor Morphology and Metal Location for Enhancing Solar Energy Conversion. *Small*. **2017**, *13*, 1602629; (b) Cozzoli, P. D.; Curri, M. L.; Giannini, C.; Agostiano, A. Synthesis of TiO_2–Au Composites by Titania–Nanorod–Assisted Generation of Gold Nanoparticles at Aqueous/Nonpolar Interfaces. *Small.* **2006**, *2*, 413–421; (c) Debangshi, A.; Thupakula, U.; Khan, A. H.; Kumar, G. S.; Sarkar, P. K.; Acharya, S. Probing Local Electronic Structures of Au–PbS Metal–Semiconductor Nanodumbbells. *ACS Appl. Nano Mater*. **2018**, *1*, 2104–2111; (d) Liu, Q.; Shang, Q.; Khalil, A.; Fang, Q.; Chen, S.; He, Q.; Xiang, T.; Liu, D.; Zhang, Q.; Luo, Y.; Song, L. *In situ* Integration of a Metallic 1T-MoS_2/CdS Heterostructure as a Means to Promote Visible–Light–Driven Photocatalytic Hydrogen Evolution. *ChemCatChem* **2016**, *8*, 2614–2619; (e) Xiang, Q.; Cheng, F.; Lang, D. Hierarchical Layered WS_2/Graphene–Modified CdS Nanorods for Efficient Photocatalytic Hydrogen Evolution. *ChemSusChem* **2016**, *9*, 996–1002; (f) Bera, R.; Kundu, S.; Patra, A. 2D Hybrid Nanostructure of Reduced Graphene Oxide–CdS Nanosheet for Enhanced Photocatalysis. *ACS Appl. Mater. Interfaces* **2015**, *7*, 13251–13259; (g) Liang, S.; Han, B.; Liu, X.; Chen, W.; Peng, M.; Guan, G.; Deng, H.; Lin, Z. 3D Spatially Branched Hierarchical Z–Scheme CdS–Au Nanoclusters–ZnO Hybrids with Boosted Photocatalytic Hydrogen Evolution. *J. Alloys Compd*. **2018**, *754*, 105–113; (h) Chen, D.; Wang, A.; Li, H.; Galán, L. A.; Su, C.; Yin, Z.; Massi, M.; Suvorova, A.; Saunders, M.; Li, J.; Sitt, A.; Jia, G. Colloidal Quasi-One-Dimensional Dual Semiconductor Core/Shell Nanorod Couple Heterostructures with Blue Fluorescence. *Nanoscale* **2019**, *11*, 10190–10197; (i) Dilsaver, P. S.; Reichert, M. D.; Hallmark, B. L.; Thompson, M. J.; Vela, J. Cu_2ZnSnS_4–Au Heterostructures: Toward Greener Chalcogenide-Based Photocatalysts. *J. Phys. Chem. C* **2014**, *118*, 21226–21234; (j) Xu, B.; He, P.; Liu, H.; Wang, P.; Zhou, G.; Wang, X. A 1D/2D Helical CdS/$ZnIn_2S_4$ Nano-Heterostructure. *Angew. Chem. Int. Ed*. **2014**, *53*, 2339–2343.

[28] Zhuang, T.; Liu, Y.; Sun, M.; Jiang, S.; Zhang, M.; Wang, X.; Zhang, Q.; Jiang, J.; Yu, S. A Unique Ternary Semiconductor–(Semiconductor/Metal) Nano–Architecture for Efficient Photocatalytic Hydrogen Evolution. *Angew. Chem. Int. Ed*. **2015**, *127*, 11657–11662.

[29] (a) Ye, C.; Regulacio, M. D.; Lim, S. H.; Li, S.; Xu, Q.; Han, M. Alloyed ZnS–$CuInS_2$ Semiconductor Nanorods and Their Nanoscale Heterostructures for Visible–Light–Driven Photocatalytic Hydrogen Generation. *Chem. - Eur. J*. **2015**, *21*, 9514–9519; (b) Ye, C.; Regulacio, M. D.; Lim, S. H.; Xu, Q.-H.; Han, M.-Y. Alloyed $(ZnS)_x(CuInS_2)_{1-x}$ Semiconductor Nanorods: Synthesis, Bandgap Tuning and Photocatalytic Properties. *Chem. - Eur. J.* **2012**, *18*, 11258–11263.

[30] Ben-Shahar, Y.; Scotognella, F.; Waiskopf, N.; Kriegel, I.; Conte, S. D.; Cerullo, G.; Banin, U. Effect of Surface Coating on the Photocatalytic Function of Hybrid CdS–Au Nanorods. *Small* **2015**, *11*, 462–471.

[31] (a) Feng, Y.; Shi, X.; Wang, X.; Lee, H.; Liu, J.; Qu, Y.; He, W.; Kumar, S. S.; Kim, B. H.; Ren, N. Effects of Sulfide on Microbial Fuel Cells with Platinum and Nitrogen-Doped Carbon Powder Cathodes. *Biosens. Bioelectron.* **2012**, *35*, 413–415; (b) Berr, M. J.; Vaneski, A.; Mauser, C.; Fischbach, S.; Susha, A. S.; Rogach, A. L.; Jäckel, F.; Feldmann, J. Delayed Photoelectron Transfer in Pt–Decorated CdS Nanorods under Hydrogen Generation Conditions. *Small* **2012**, *8*, 291–297; (c) Wu, K.; Zhu, H.; Lian, T. Ultrafast Exciton Dynamics and Light–Driven H_2 Evolution in Colloidal Semiconductor Nanorods and Pt–Tipped Nanorods. *Acc. Chem. Res*. **2015**, *48*, 851–859.

[32] Wu, K.; Chen, Z.; Lv, H.; Zhu, H.; Hill, C. L.; Lian, T. Hole Removal Rate Limits Photodriven H_2 Generation Efficiency in CdS–Pt and CdSe/CdS–Pt Semiconductor Nanorod–Metal Tip Heterostructures. *J. Am. Chem. Soc*. **2014**, *136*, 7708–7716.

[33] Berr, M. J.; Wagner, P.; Fischbach, S.; Vaneski, A.; Schneider, J.; Susha, A. S.; Rogach, A. L.; Jäckel, F.; Feldmann, J. Hole Scavenger Redox Potentials Determine Quantum Efficiency and Stability of Pt–Decorated CdS Nanorods for Photocatalytic Hydrogen Generation. *Appl. Phys. Lett*. **2012**, *100*, 223903.

[34] (a) Plante, I. J.; Teitelboim, A.; Pinkas, I.; Oron, D.; Mokari, T. Exciton Quenching Due to Copper Diffusion Limits the Photocatalytic Activity of CdS/Cu_2S Nanorod Heterostructures. *J. Phys. Chem. Lett*. **2014**, *5*, 590–596; (b) Ruberu, T. P. A.; Vela, J. Expanding the One-Dimensional CdS–CdSe Composition Landscape: Axially Anisotropic $CdS_{1-x}Se_x$ Nanorods. *ACS Nano* **2011**, *5*, 5775–5784; (c) Kumar, S.; Jones, M.; Lo, S. S.; Scholes, G. D. Nanorod Heterostructures Showing Photoinduced Charge Separation. *Small* **2007**, *3*, 1633–1639; (d) Grennell, A. N.; Utterback, J. K.; Pearce, O. M.; Wilker, M. B.; Dukovic, G. Relationships between Exciton Dissociation and Slow Recombination within ZnSe/CdS and CdSe/CdS Dot–in–Rod Heterostructures. *Nano Lett.* **2017**, *17*, 3764–3774; (e) Kudera, S.; Carbone, L.; Casula, M. F.; Cingolani, R.; Falqui, A.; Snoeck, E.; Parak, W. J.; Manna, L. Selective Growth of PbSe on One or Both Tips of Colloidal Semiconductor Nanorods. *Nano Lett.* **2005**, *5*, 445–449; (f) Shen, S.; Zhang, Y.; Peng, L.; Du, Y.; Wang, Q. Matchstick-Shaped Ag_2S–ZnS Heteronanostructures Preserving both UV/Blue and Near-Infrared Photoluminescence. *Angew. Chem. Int. Ed.* **2011**, *123*, 7253–7256; (g) Yu, X.; Shavel, A.; An, X.; Luo, Z.; Ibáñez, M.; Cabot, A. Cu_2ZnSnS_4-Pt and Cu_2ZnSnS_4-Au Heterostructured Nanoparticles for Photocatalytic Water Splitting and Pollutant Degradation. *J. Am. Chem. Soc.* **2014**, *136*, 9236–9239.

[35] Zhang, K.; Kim, J. K.; Ma, M.; Yim, S. Y.; Lee, C.; Shin, H.; Park, J. H. Delocalized Electron Accumulation at Nanorod Tips: Origin of Efficient H_2 Generation. *Adv. Funct. Mater*. **2016**, *26*, 4527–4534.

[36] Tang, M. L.; Grauer, D. C.; Lassalle-Kaiser, B.; Yachandra, V. K.; Amirav, L.; Long, J. R.; Yano, J.; Alivisatos, A. P. Structural and Electronic Study of an Amorphous MoS_3 Hydrogen-Generation Catalyst on a Quantum-Controlled Photosensitizer. *Angew. Chem. Int. Ed.* **2011**, *123*, 10385–10389.

[37] Kameyama, T.; Koyama, S.; Yamamoto, T.; Kuwabata, S.; Torimoto, T. Enhanced Photocatalytic Activity of Zn–Ag–In–S Semiconductor Nanocrystals with a Dumbbell–Shaped Heterostructure. *J. Phys. Chem. C* **2018**, *122*, 13705–13715.

[38] Manzi, A.; Simon, T.; Sonnleitner, C.; Döblinger, M.; Wyrwich, R.; Stern, O.; Stolarczyk, J. K.; Feldmann, J. Light-Induced Cation Exchange for Copper Sulfide Based CO_2 Reduction. *J. Am. Chem. Soc.* **2015**, *137*, 14007–14010.

[39] Pan, R.; Liu, J.; Li, Y.; Li, X.; Zhang, E.; Di, Q.; Su, M.; Zhang, J. Electronic Doping–Enabled Transition from n– to p–Type Conductivity Over Au@CdS Core–Shell Nanocrystals Toward Unassisted Photoelectrochemical Water Splitting. *J. Mater. Chem. A* **2019**, *7*, 23038–23045.

[40] Ma, X.; Guo, S.; Shen, J.; Chen, Y.; Chen, C.; Sun, L.; Zhang, X.; Ruan, S. Synthesis and Enhanced Gas Sensing Properties of Au-Nanoparticle Decorated CdS Nanowires. *RSC Adv*. **2016**, *6*, 70907–70912.

[41] Waiskopf, N.; Ben-Shahar, Y.; Galchenko, M.; Carmel, I.; Moshitzky, G.; Soreq, H.; Banin, U. Photocatalytic Reactive Oxygen Species Formation by Semiconductor–Metal Hybrid Nanoparticles. Toward Light–Induced Modulation of Biological Processes. *Nano Lett*. **2016**, *16*, 4266–4273.

Manuscript received: March 30, 2023
Manuscript revised: May 28, 2023
Manuscript accepted: June 23, 2023
Accepted manuscript online: June 27, 2023
Version of record online: August 22, 2023

